Arrhythmia Management: Control of Alternans & *VIEgram* for analysis and visualization of electrograms to aid Atrial Fibrillation Treatment

A THESIS
SUBMITTED TO THE FACULTY OF THE
UNIVERSITY OF MINNESOTA
BY

Sanket Yograj Thakare

IN PARTIAL FULFILLMENT OF THE REQUIREMENTS
FOR THE DEGREE OF
MASTER OF SCIENCE

Advisor: Dr. Alena Talkachova

July 2020

Acknowledgements

I am extremely indebted to my advisor Dr. Alena Talkachova for giving me an opportunity to explore cardiac electrophysiology. Her expertise, continuous guidance, and unwavering support helped me a lot during my research.

I would like to thank my committee members Dr. Paul Iaizzo and Dr. Hubert Lim for their support, guidance, and research insights. I am also grateful to my labmates, Vasanth Ravikumar, Xiangzhen Kong, Jieun Lee, Preethy P., Yugene Guo, Brett Levac, and Samuel Newell for all the help and support.

Table of Contents

List of Tables

List of Figures

CHAPTER 1: INTRODUCTION

1.1 Overview of Cardiac Electrophysiology and Arrhythmias

The heart is one of the most complex and vital organs contained within the human body. Each day, the average human heart beats about 100,000 times and pumps around 2,000 gallons of blood through the body. Thus, the heart, which consists of cardiac muscle, is said to be the hardest working muscle in the body. Cardiac muscle, an involuntary muscle that constitutes the main tissue of the walls of the heart, controls the contractions of the heart. The intrinsic conduction system of the heart which is a group of specialized cardiac cells sends electrical signals to these cardiac muscles causing it to contract.

In a healthy heart, the electrical impulse emanates from the sinoatrial (SA) node, the heart's own natural pacemaker (see Fig. 1.1 (a)). These pacemaker cells cause spontaneous depolarizations and are responsible for generating the normal cardiac rhythm. After initial excitation at SA node, depolarization spreads throughout the atria and causes it to contract. Then, the electrical excitation travels through the atrioventricular (AV) node which takes some time thereby providing enough time for the ventricles to fill up. From the AV node, which serves as the electrical connection between the atria and the ventricles, the electrical excitation spreads throughout the ventricles through Purkinje fibers via the Bundle of His and thus causes the ventricles

to contract. For the heart to function properly, the atria and ventricles should contract in a coordinated fashion.

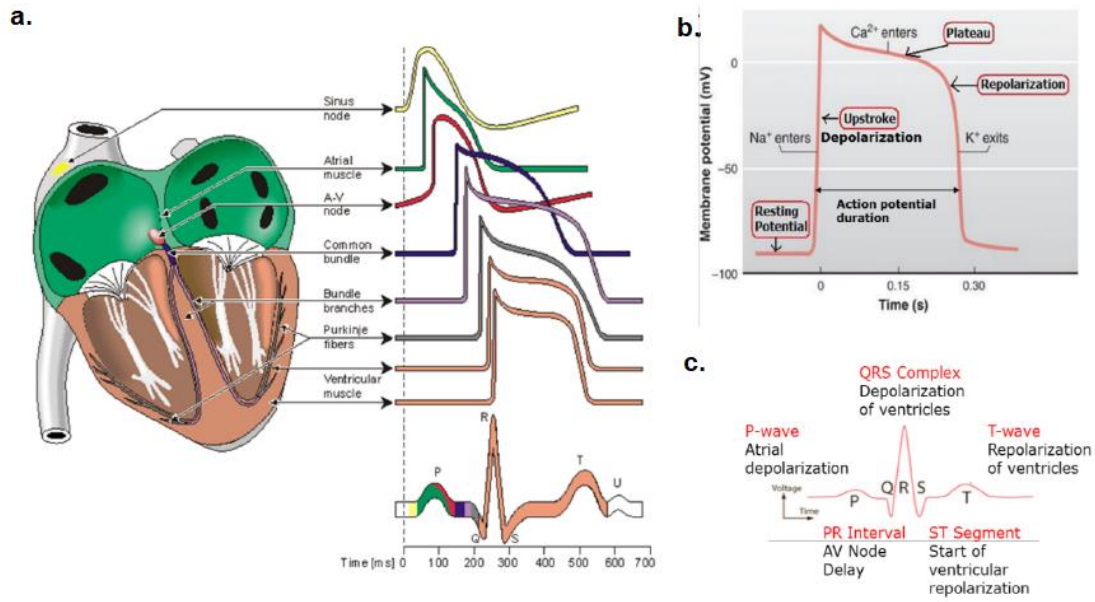

Figure 1.1: (a) [Adapted from from (Malmivuo and Plonsey, 'Bioelectromagnetism')] Electrophysiology of the heart with voltage or action potential waveforms for each region shown distinctly along with cumulative ECG trace. (b) Ventricular action potential trace showing different phases of activation. (c) Correlation between ECG trace and activation of different regions of the heart

Cardiomyocytes are cells that make up the cardiac muscle. The contraction of the heart is a phenomenon that is brought about by a well-timed summation of single cardiomyocyte contractions. The contraction of each myocyte is triggered by the electrical wave of excitation that originates from the SA node. Each time a myocyte is triggered, the properties of transmembrane ion channels (e.g. sodium, potassium, calcium, etc.) change and a complex movement of ions in and out of the cell takes place,

thereby causing a cyclic change in the membrane potential. This sequence of changes in the membrane potential is known as the action potential. The action potential of one myocyte will act as the stimulus to surrounding cells through gap junctions and diffusion, thus, eliciting an action potential in downstream cells in the conduction system. This process is repeated until the electrical signal propagates through the entire heart causing it to contract. Fig. 1.1 depicts the elicited action potentials by cardiac cells corresponding to different regions of the heart and its correlation to the average activity recorded on an electrocardiogram (ECG).

Arrhythmia is an abnormal heart rhythm and can be caused by irregularities in cardiac electrical activity. Some common types of arrhythmias are described in Table 1.1. Arrhythmias are exhibited as unstable variations in cardiac cellular electrical impulses, also known as action potential durations (APDs). An alarming number of people have been reported to manifest sudden cardiac death (SCD) as the first symptom of cardiac arrhythmias, leading to an estimated 600,000 fatalities per year. Efforts for decreasing this substantial number have led to the proliferation of medical devices and researches aimed at restoring the normal electrical activity in diseased and failing hearts.

Type of Arrhythmia	**Description**
Ventricular Tachycardia (VT)	Regular but rapid heart rhythm of the ventricles, resulting in abnormally high heart rates.

Ventricular Fibrillation (VF)	Irregular, chaotic, and rapid ventricular rhythm that causes the ventricles to quiver. This results in the heart not able to contract or pump blood.
Atrial Fibrillation (AF)	Irregular, chaotic rhythm of the atria. This causes no atrial hemodynamic input to the ventricles and the stasis of blood in the atria can result in clot formation and stroke.
Atrial Flutter or Tachycardia	Abnormally high atrial rate.
Bradycardia	Slow heart rhythm.

Table 1.1 Common examples of cardiac arrhythmias

1.2 Spatial and Temporal Complexity of Arrhythmia

The heart is regulated by multiple factors in a nonlinear fashion at different levels both in time and space, and thus can be viewed as a nonlinear spatially extended dynamical system, with arrhythmias being one of the characteristic behaviors of such a system. Arrhythmia is a multiscale problem that is influenced by physiological factors at all levels: molecular, sub-cellular, cellular, tissue, and organ [1]. At molecular and sub-cellular levels, the complex intracellular signaling regulates the properties of ionic channels and intracellular Ca^{2+} cycling dynamics. The cardiac AP, elicited by myocytes at the cellular level, is a result of the ionic currents flowing through the ionic channels whose gating kinetics can be highly nonlinear. At the tissue and organ levels, the

complex nonlinear cell-to-cell communication, a molecular mechanism by which AP spreads from cell to cell through gap junctions, leads to changes in electrophysiological properties at the cellular level, including AP, Ca^{2+} cycling, automaticity, early (EAD) and delayed (DAD) afterdepolarization, excitability, refractoriness, spatial alternans, etc., which altogether impact arrhythmias. Hence, in overall, the dynamics of the heart can be described as a macroscopic behavior of many interacting material entities [2].

Several deviations from the spatio-temporal organization of electrical activity in the heart might occur, leading to various types of arrhythmias: focal excitation, anatomical re-entry, and functional re-entry. Therefore, arrhythmia is not a property of the individual cells or channel proteins; it is rather an emergent phenomenon of the spatially extended tissue. In addition to dynamic factors, pre-existing factors such as various structural and electrophysiological heterogeneities like scars, fibrosis, electrical channel and gap junction remodeling, transmural and apex-to base heterogeneity etc., create a dispersion of refractoriness and excitability, which affect tissue substrate, thus affecting arrhythmogenesis.

Arrhythmia management - prediction, prevention and control of arrhythmias, is difficult mainly due to its spatiotemporal complexity and the poor understanding of mechanisms causing them. Therapies for managing arrhythmias can be focused at two macroscopic levels, namely cellular level and tissue/organ level. At cellular level, arrhythmias can be prevented by reviving the abnormal electrophysiological function of myocytes and thus preventing it from getting evolved into dangerous reentrant arrhythmias at the tissue level. For example, ventricular arrhythmias can be prevented by employing a pacing protocol to control cardiac alternans at cellular level. Whereas

at tissue/organ level, the arrhythmia which is already present can be controlled. For example, the catheter ablation procedure, a procedure where tissue causing abnormal electrical activity is ablated, is used to treat AF on an organ level to return the heart back to its normal sinus rhythm. Also, at an organ level we can deal with the pre-existing factors contributing to arrhythmogenesis. Furthermore, a visualization of all the manifestations of arrhythmias on an organ level (3D models of a patient's heart) will not only help in understanding the complex spatiotemporal mechanisms behind them but will also facilitate the development of new techniques to treat them.

1.3 Cardiac Alternans

Cardiac alternans is an alternation of APD between long and short values. Alternans desynchronizes depolarization, increases the dispersion of refractoriness, and creates a substrate for arrhythmias [3]. In the ventricles, cardiac alternans manifests itself as T-wave alternans in an ECG and is believed to be a direct precursor to ventricular fibrillation (VF) [4]–[7]. VF can then lead to SCD which is one of the leading causes of natural death in the US. Previous studies have established a plausible link between alternans and ventricular arrhythmias suggesting that elimination of alternans could lead to the prevention of VF and eventual arrhythmias in the heart [6], [8]–[10].

The heart comprises excitable cells that elicit an action potential in response to a stimulus. The basic cycle length (BCL) of the cardiac action potential can be split up into two main components: the action potential duration (APD) and the diastolic interval (DI). Under normal pacing rate, cardiac cells elicit action potentials upon electrical stimulation, with all APD being equal, named 1:1 response (see Fig. 1.2(a)). When the

pacing rate is increased to a sufficiently high rate, the normal 1:1 response can become unstable, and the APD alternates between short and long values resulting in an alternans [8] (see Fig. 1.2(b)). Electrical restitution theory explains the cardiac dynamics through the dependence of APD on the preceding DI (cardiac relaxation phase). However, under periodic pacing where BCL is kept constant, this dependency of APD on preceding DI leads to inherent feedback which makes the heart more susceptible to electrical destabilization and formation of alternans.

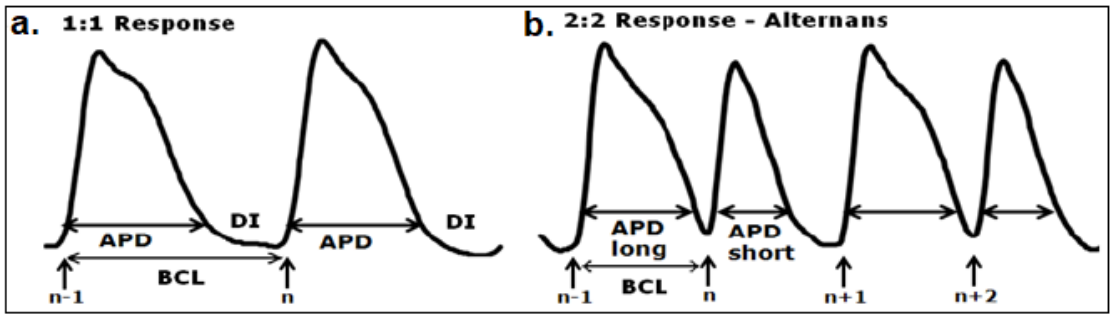

Figure 1.2: Action Potential Traces showing (a) Constant APD at higher BCL (normal pacing rate); (b) APD alternans at lower BCL (higher pacing rate)

Currently, cardiac pacemakers are being used as a therapeutic device to regulate the heart function and rhythm in patients with abnormal cardiac electrical activity. However, most of the pacemakers still use periodic stimulation to restore normal cardiac rhythm, potentially promoting electrical instability in the heart. Recently, a constant DI pacing protocol was proposed for preventing alternans formation by eliminating the feedback between APD and preceding DI [11]. Since the implementation of constant DI pacing has practical limitations as it requires the real-time recording of transmembrane voltage, an ECG-based approach was proposed which uses TR interval, an indirect

measure of the global DI relaxation period [12]. It was shown to prevent alternans formation in isolated Langendorff-perfused rabbit hearts. However, the efficacy of "local" constant DI pacing vs "global" constant TR pacing in preventing the alternans formation has never been investigated. This leads to the first aim of my thesis - **to implement the ECG-based constant TR pacing protocol, a global pacing mechanism, on a human ventricular tissue model and study its efficacy in controlling the alternans when compared to constant DI pacing, a localized pacing mechanism.**

1.4 Atrial fibrillation

Atrial fibrillation (AF) is the most common sustained arrhythmia. In AF, the atria contract rapidly and irregularly due to the abnormalities in the spatio-temporal organization of atria's electrical activity. According to an estimate in 2014, 2.7 to 6.1 million people in the United States are afflicted by AF. AF is the most prevalent arrhythmia in the United States and is associated with an increased risk of stroke [13]. In Fig. 1.3 (a), a normal heart is shown where yellow pathways represent the intrinsic conduction system of the heart, and in Fig. 1.3 (b), a heart with AF is shown. It can be noticed that there are several sites in atria that are radiating abnormal electrical activities which then causes rapid irregular atrial contractions and thus these sites can also be referred to as AF causing sites. Besides pharmacological treatment, catheter ablation has become the most popular treatment for AF in recent times. In catheter ablation procedure, the clinicians create a lesion at AF causing sites thus making it unable to conduct. By ablating all such sites, the heart returns back to its normal rhythm.

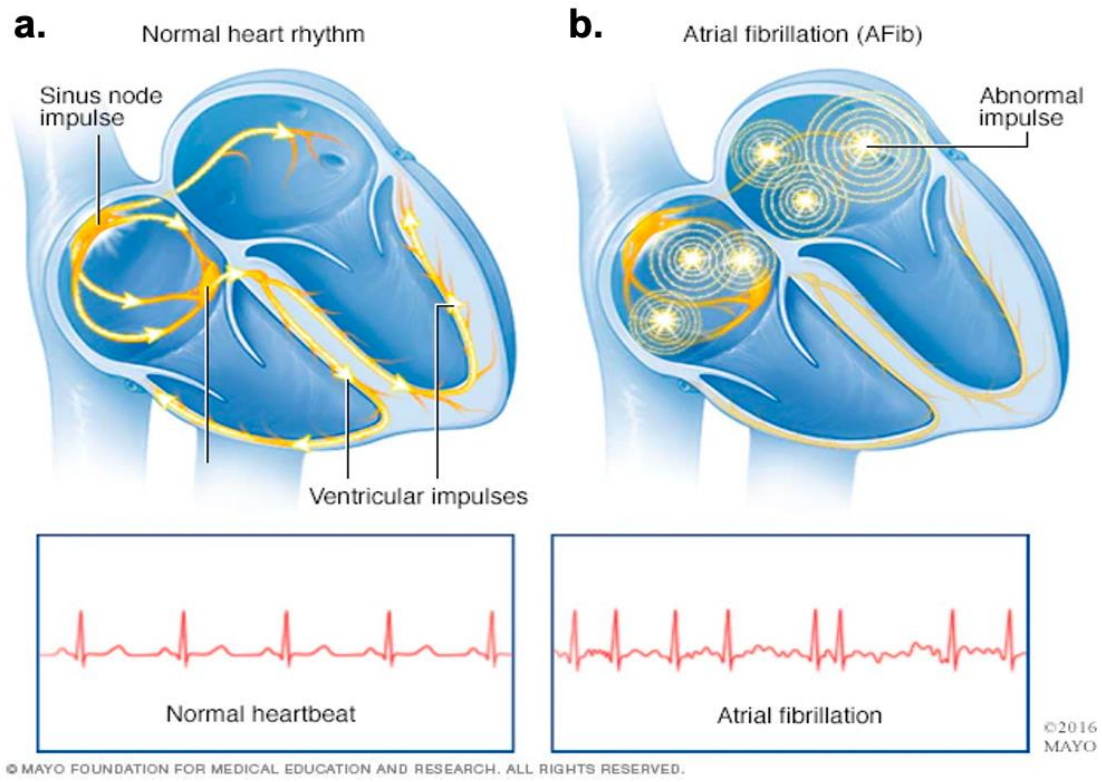

Figure 1.3: (a) A conduction system of normal heart, (b) A heart with atrial fibrillation where electrical signals fire from multiple locations in the atria, causing them to beat irregularly and rapidly.

During electrophysiological (EP) studies, intracardiac electrograms (iEGMs) are recorded from various endocardial sites using the multipolar diagnostic catheters. Electroanatomical mapping (EAM) systems like CARTO, EnSite Precision, RHYTHMIA, etc., are then used to map these recorded iEGMs on a patient's 3D heart model which provides the basis for diagnosis and guiding the ablation procedure. Thus, for the success of the ablation procedure, the detection of AF causing sites is very crucial and has been a research topic for many. The researchers use these recorded iEGMs to automate the detection of target sites for ablation. However, these developed analyses

cannot be installed and tested on the proprietary EAM systems. Thus, the development of novel techniques to automate the analysis of iEGMs has been hampered due to the restricted access to the clinically used proprietary EAM systems. This indicates a need for visualization software that allows the rapid implementation of newly developed analysis techniques, verification of their functionality, and suitable visualizations for discussion in the clinical environment. This leads to the second aim of the thesis - **to develop a visualization software that allows researchers to visualize the results of the various iEGMs analysis on a patient-specific 3D atria model**. Such software will eliminate the dependency on the proprietary EAM systems, thereby making the process of retrospective mapping extremely convenient and time efficient.

1.5 Thesis Organization

Chapter 2 describes the implementation of an ECG-based constant TR pacing in a 1D numerical model of human ventricular tissue. Details of the numerical investigations performed, and the results are also provided. The goal of this project was to compare the efficacy of constant TR pacing in preventing the onset of alternans with the constant DI pacing.

Chapter 3 discusses the development of open-source 3D visualization software, *VIEgram*. Its flexibility in terms of performing different iEGMs analysis and their visualization on a patient's 3D heart model is explained in detail.

Chapter 4 summarizes the work completed as part of this thesis by highlighting the major findings and discussing the possible future directions.

CHAPTER 2: GLOBAL VERSUS LOCAL CONTROL OF CARDIAC ALTERNANS

(The work in this chapter has been accepted for publication as Sanket Thakare, Joseph Mathew, Sharon Zlochiver, Xiaopeng Zhao, Elena G. Tolkacheva, "Global versus Local Control of Cardiac Alternans in a 1D Numerical Model of Human Ventricular Tissue", Chaos: An Interdisciplinary Journal of Nonlinear Science, 2020)

Author Contributions:

Concept was developed by E.G.T. and X.Z. Pacing protocol was implemented by J.M. and S.T. on the numerical model provided by S.Z. Data was analyzed by S.T. and J.M., and prepared for publication by S.T. and E.G.T.

Abstract

Cardiac alternans is a proarrhythmic state in which the action potential duration (APD) of cardiac myocytes alternate between long and short values, and often occurs under conditions of rapid pacing of cardiac tissue. In the ventricles, alternans is especially dangerous due to the life-threatening risk of developing arrhythmias, such as ventricular fibrillation. Alternans can be formed in periodically paced tissue as a result of pacing itself. Recently, it has been demonstrated that this pacing-induced alternans can be prevented by performing constant diastolic interval (DI) pacing, in which DI is independent of APD. However, constant DI pacing is difficult to implement in experimental settings since it requires the real-time measurement of APD. A more practical way was proposed based on electrocardiogram (ECG), which gives an indirect measure of the global DI relaxation period through the TR interval assessment. Previously, we demonstrated that constant TR pacing prevented alternans formation in isolated Langendorff-perfused rabbit hearts. However, the efficacy of "local" constant DI pacing vs "global" constant TR pacing in preventing the alternans formation has never been investigated. Thus, the purpose of this study was to implement an ECG-based constant TR pacing in a 1D numerical model of human ventricular tissue and to compare the dynamical behavior of the cardiac tissue with that resulted from a constant DI pacing. The results showed that both constant TR and constant DI pacing prevented the onset of alternans until lower basic cycle length (BCL) when compared to periodic pacing. For longer cable lengths, constant TR pacing was shown to exhibit greater control on alternans than constant DI pacing.

Cardiac alternans, an alternation of APD between long and short values, may lead to fatal cardiac arrhythmias and sudden cardiac death [14]. A large portion of alternans research is based on the restitution theory, which proposes that under periodic pacing at a constant basic cycle length (BCL), the subsequent APD is a function of the previous DI. Based on this theory, a constant DI pacing protocol would eliminate the feedback between the BCL and APD seen with periodic pacing and prevent alternans onset. However, the implementation of constant DI pacing has practical limitations as it requires the real-time recording of transmembrane voltage. Here, we have implemented an ECG-based constant TR pacing, a global pacing mechanism, on a human ventricular tissue model to study its efficacy in controlling the alternans when compared to constant DI pacing.

2.1 Introduction

Cardiac alternans in the ventricles of the heart manifests itself as T-wave alternans (TWA) in an electrocardiogram (ECG), which is a clinical indicator for cardiac arrhythmias like ventricular fibrillation and sudden cardiac death [5], [14]–[16]. Since the alternans is linked to increased susceptibility to ventricular arrhythmias, alternans prevention and/or control have been the subject of many numerical and experimental research studies [11], [16]–[24]. Under normal pacing rate, cardiac cells in the human heart elicit action potentials upon electrical stimulation [25], with all action potential durations (APD) being equal, named 1:1 (or period-1) response (see Fig. 2.1(a)). When the pacing rate is increased to a sufficiently high rate, the normal 1:1 response can become unstable, and the APD alternates between short and long values resulting in an

alternans [11] (period-2 response, see Fig. 2.1(b)). Electrical restitution theory [26] expresses cardiac dynamics through the dependence of APD_{n+1} on the previous DI_n as

$$APD_{n+1} = f(DI_n), \tag{1}$$

where DI is the diastolic interval, n is the stimulus number, and f is the restitution curve. If the cardiac cell is paced periodically, the following relation occurs:

$$BCL_n = APD_n + DI_n, \tag{2}$$

where BCL is the basic cycle length, i.e. the interval between two stimuli (see Fig. 2.1), which is inversely proportional to pacing rate. During periodic pacing, the BCL is constant, i.e., BCL_n=BCL=*const*, and the DI_n is not independent, but is determined by the following relation

$$DI_n = BCL - APD_n . \tag{3}$$

It has been demonstrated that increasing pacing at a small BCL may destabilize the 1:1 response and lead to the formation of alternans (Fig. 2.1(b)) [11], [18].

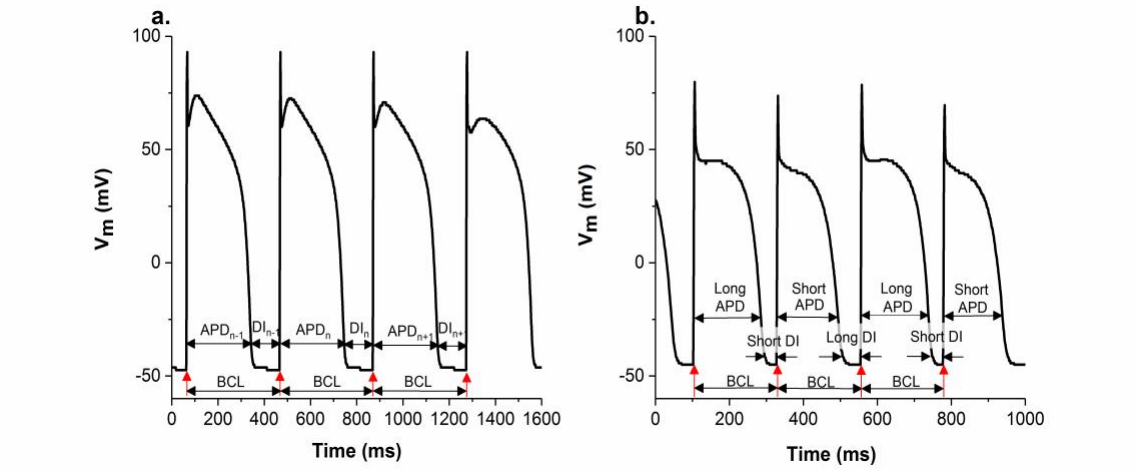

Figure 2.1: Action potential traces and relationship between APD, DI and BCL for (a) normal 1:1 response and (b) alternans (period-2 rhythm). Stimulation pulses are indicated by red arrows.

Several mechanisms were proposed for alternans control [9], [19], [22], [24], [27]–[30]. Feedback control of cardiac alternans was first proposed in [9], [22], where alternans was suppressed by varying the pacing interval by an amount proportional to the difference between the APD from the two previous intervals. However, this control scheme is spatially limited as it is effective only for small amplitude of alternans, and control became attenuated as amplitude increased [31]. Dubljevic et al. [27] discussed a feedback control method to suppress alternans both spatially and temporally in an extracted rabbit heart and a cable of cardiac cells. Since the numerical simulation and experiment were based on a single measurement, it could only stabilize a single unstable mode. As unstable mode increases with an increase in pacing frequency or tissue length, such a feedback control failed to stabilize the alternans in a cable tissue greater than 1 cm and thus limits its applicability to the cardiac tissue of realistic dimensions. Also, chaos control [19], [28], [29] and adaptive control [30] schemes were used to prevent alternans. However, such control is effective only in small size tissue or in long Purkinje fibers, and its efficacy is significantly limited in more spatiotemporally complex two-dimensional (2D) settings. These control algorithms used periodic pacing where the duration between consecutive stimuli (i.e., *BCL*) is constant from beat-to-beat. During such periodic pacing, there is a partial dependence of the *DI* on the preceding *APD* that can subsequently destabilize the normal cardiac rhythms [11], [18].

Most of the alternans control mechanisms proposed over the past decades are based on beat-to-beat adjustments to the BCL_n [11], [12], [17], [19], [20]. Recently, we proposed to use a constant DI protocol for prevention of alternans formation [12]. This protocol keeps DI_n=*const* in Eq. (3), thus eliminating the instabilities that can arise in

the system through changes in APD_n. It was demonstrated that constant DI pacing was superior in preventing alternans formation when compared to periodic (or so-called constant BCL) pacing in a numerically simulated 1D ventricular fiber [16]. Based on these results, Kulkarni et al. [12] experimentally implemented a constant DI pacing protocol in an isolated perfused rabbit heart by developing a closed-loop system to detect T-waves from real-time ECG signal on a beat-by-beat basis. After detecting the T-wave, the heart was paced after a predefined duration (constant TR interval), which was considered in [12] to be equivalent to the DI.

Despite the strong analogy between constant DI and constant TR controls, the two protocols are fundamentally different (see Fig. 2.2). Indeed, DI represents the "local" measurements that can only refer to a single cell, while ECG is a "global" or averaged measure of electrical activity. Intuitively, the constant TR pacing may be regarded as a "globalized" version of the constant DI pacing. Nevertheless, it is unclear whether such interpretation and difference between constant DI and constant TR protocols affect their ability to prevent alternans.

Thus, the aim of this paper was to compare the performance of the two protocols using a numerical model of a human ventricular fiber and assess their efficacy in preventing alternans at different cable lengths. At higher pacing rates, the intracellular calcium cycling of cardiac myocytes can contribute to the formation of alternans due to the inconsistency between calcium uptake and calcium release from the sarcoplasmic reticulum [32]. The membrane voltage and intracellular calcium transients are highly interdependent and bidirectionally coupled [33] via sodium-calcium exchanger. Thus,

we also examined a contribution of voltage-calcium coupling to alternans instabilities under constant TR pacing.

2.2 Methods

2.2.1 Numerical Simulations

The electrical propagation along a 1D human ventricular fiber was simulated as described in Ref. 11. The 1D fiber was surrounded by non-conducting boundary cells to eliminate boundary effects. The transmembrane voltages (V_m) of each cell were calculated using the following reaction-diffusion partial differential equation for myocytes under the mono-domain approximation:

$$\frac{\partial V_m}{\partial t} = -\frac{(I_{ion} + I_{stim})}{C_m} + \nabla \cdot (D\nabla V), \quad (4)$$

where C_m [μF/cm^2] is the membrane capacitance per unit area, I_{stim} [μA/cm^2] is the external stimulation current, and D [mm^2/ms] is the diffusion coefficient for electrical propagation and was set to 0.12 mm^2/ms. I_{ion} represents the ionic currents which were calculated using the Ten Tusscher and Panfilov kinetic model for a human ventricular myocyte [12]. Eq. (4) was solved by using forward Euler integration at a time step of 0.0075 ms for all simulations. The cable length L was varied from 1 cm to 6 cm, which corresponds to the average dimension of the human end-diastolic left ventricle being 3.6-5.6 cm [7]. L was varied by changing the number of cells, where each cell was 0.01 cm long.

The parameters to maintain an APD restitution curve slope of 1.8 were set to the following values for all simulations, as described in Ref. 5: G_{Kr} = 0.172 nS/pF, G_{Ks} =

0.441 nS/pF, G_{pCa} = 0.8666 nS/pF, G_{pK} = 0.00219 nS/pF, and $\tau_f = 2 \times \tau_f$(reference), where Gkr, GKs, GpCa, and GpK are the maximal conductance for the IKr, IKs, IpCa, and IpK currents, respectively, and τ_f is the calcium f-gate time constant for positive voltages.

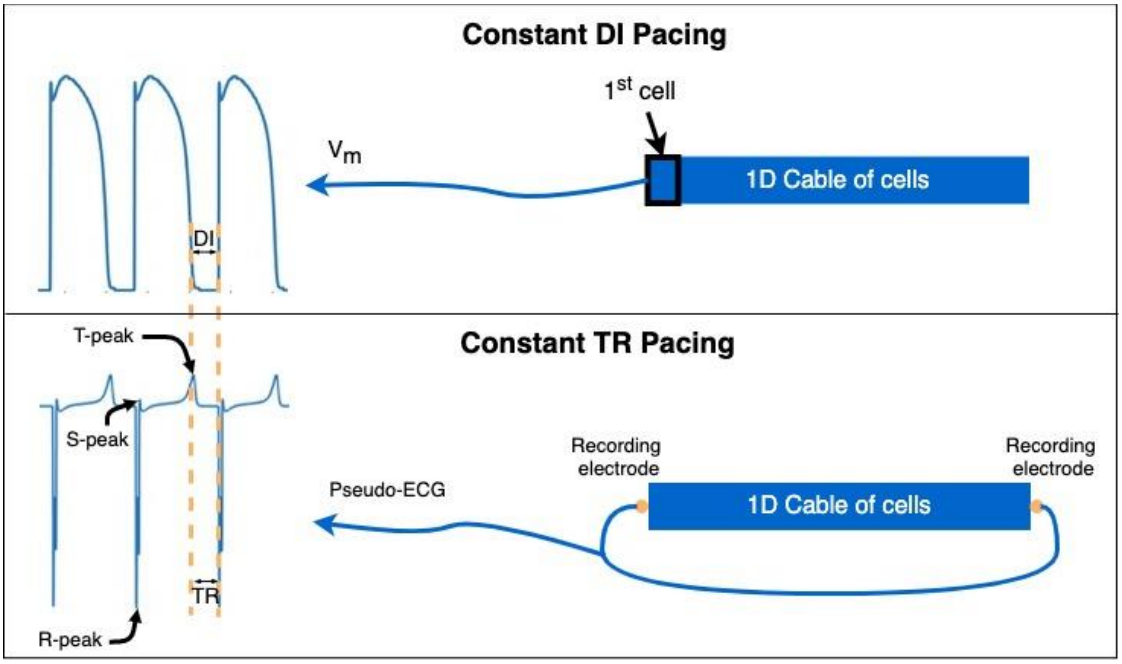

Figure 2.2: Comparison between constant DI (top) and constant TR (bottom) pacing protocols. Constant DI pacing measures the transmembrane potential of a single cell in a cable, while constant TR pacing uses electrodes to record ECG from the electrical activity of all the cells in a cable. TR interval of pseudo-ECG can be seen to align with DI of transmembrane voltage (V_m) trace.

2.2.2 Pacing Protocols

Constant DI pacing protocol was implemented as described in [11]. Specifically, after an initial stimulus, APD at 90% repolarization (APD_{90}) was calculated, and the next stimulus was applied after a fixed time interval (i.e., constant DI) from APD_{90}. A

set of 50 stimuli were applied for a specific DI (to achieve a steady-state), and then the DI was gradually decreased according to the following equation:

$$\mathrm{DI(i)} = \ 125 - (i-1) \ \times \ 5; \ i \geq 1 \, , \tag{5}$$

where *i* is the set number. An equivalent BCL ($\mathrm{BCL_{eq}}$) was calculated as the average of the BCLs of the last two stimuli pulses (49^{th} and 50^{th}) in each pacing set.

Constant TR pacing requires a real-time pseudo-ECG calculation which was based on the following equation:

$$\Phi_e(x', y', z') = \int (-\nabla \mathrm{V_m}) \cdot \left(\nabla \frac{1}{\mathrm{r}}\right) dx \, dy \, dz \, , \tag{6}$$

where *r* is the distance from a source point to a field point. Since the present work involved a 1D fiber, the Eq. (6) was simplified to 1D and the potential was subtracted from two points:

$$\mathrm{ECG} = \Phi_e(x_\mathrm{B}) - \Phi_e(x_\mathrm{A}) = \int \left(\frac{d\mathrm{V_m}}{dx}\right) [(x - x_B)^2 + (x - x_A)^2] dx \, , \tag{7}$$

where x_A and x_B represent the positions of electrodes where $x_A < x$ and $x_B > x$ for any point *x* in the fiber. In all simulations, $x_A = 0$ and $x_B = W+2$, where W is the number of cells in the cable.

Then, real-time T-wave detection from the pseudo-ECG was implemented (see pseudo-ECG in Fig. 2.2). The state logic machine algorithm was used to detect T-waves in pseudo-ECG [34]. Once the T-wave peak was found, stimulation was applied at a fixed time interval (i.e., the constant TR) after the T-wave peak. A set of 50 stimuli were applied for a specific TR (to reach a steady-state) and after each set this specified TR interval was gradually decreased according to the following equation:

$$\mathrm{TR(i)} = \ 125 - (i-1) \ \times \ 5; \ i \geq 1, \tag{8}$$

where *i* is the set number.

A typical ECG trace along with a corresponding action potential trace is shown in Fig. 2.2 (left), and the difference between constant DI and constant TR pacing is shown in Fig. 2.2 (right). As one can see from Fig. 2.2, constant TR pacing is indeed a global version of constant DI pacing as it is based on the TR interval, a global measure of DI information.

2.2.3 Data Analysis

Bifurcation diagrams were constructed by plotting the steady-state APD_{90} values of the last two stimuli (49_{th} and 50_{th}) of each set, as a function of BCL_{eq}. The magnitude of alternans was determined as the difference in APD_{90} values of consecutive beats at any point in the cable. The threshold for alternans was set to 5 ms. Alternans was classified as spatially concordant (SCA) or spatially discordant (SDA), as described previously [11]. The onset of alternans (BCL_{onset}) was defined as the largest BCL_{eq} at which alternans occur. Conduction block (CB) threshold (BCL_{CB}) was defined as the largest BCL_{eq} under which CB occurred. The BCL_{onset} and BCL_{CB} were defined as BCL_{onset}^{DI} and BCL_{CB}^{DI} during constant DI pacing, and as BCL_{onset}^{TR} and BCL_{CB}^{TR} during constant TR pacing. In addition, we implemented constant BCL pacing, as described in Ref. 11, and we determined the BCL_{onset} (BCL_{onset}^{BCL}) under these conditions.

2.2.4 Contribution of Voltage-Calcium Coupling on the constant-TR protocol performance

To analyze the effectiveness of constant TR pacing protocol for different voltage-calcium coupling levels, we utilized the rabbit ventricular action potential model [35], which has sophisticated dynamic intracellular calcium cycling. The level of voltage-calcium coupling was modified by changing the maximal conductance of the sodium-calcium exchanger current (g_{NaCa}). g_{NaCa} was set to 4.2 μM/s for weak coupling, and 0.42 μM/s for strong coupling in comparison to its reference value of 0.84 μM/s which represents the normal coupling. A rabbit ventricular cable of L=2 cm was paced under constant TR pacing protocol for the three coupling configurations. For each simulation, APD_{90} bifurcation diagrams were constructed to determine the BCL_{onset}.

2.3 Results

2.3.1 Bifurcation Diagrams

A typical example of the bifurcation diagram constructed at x=0.5 cm in a L=2 cm cable, which was paced using constant DI protocol, is shown in Fig. 2.3(a). The onset of alternans occurred at a BCL_{onset}^{DI} = 245 ms (black vertical dashed line), while CB occurred at BCL_{CB}^{DI} = 175 ms (blue vertical dashed line). Fig. 2.3(b) shows the representative action potential trace exhibiting alternans, while Fig. 2.3(c) indicates the presence of SCA in the cable at a BCL_{eq} = 209 ms.

A similar bifurcation diagram for the same L=2 cm cable that was paced using constant a TR protocol is shown in Fig. 2.4(a). Now, the onset of alternans occurred at

BCL_{onset}^{TR} = 253.5 ms, while CB occurred at BCL_{CB}^{TR} = 174 ms. Fig. 2.4(b) shows the representative action potential trace when alternans occurred along with the corresponding pseudo-ECG trace. The TWA corresponding to APD alternans can be noticed in the pseudo-ECG trace. Fig. 2.4(c) shows the presence of SCA at BCL_{eq} = 212 ms. Thus, for L=2 cm cable, constant DI pacing (BCL_{onset}^{DI} = 245 ms) performed slightly better than constant TR pacing (BCL_{onset}^{TR} = 253.5 ms) in preventing alternans onset.

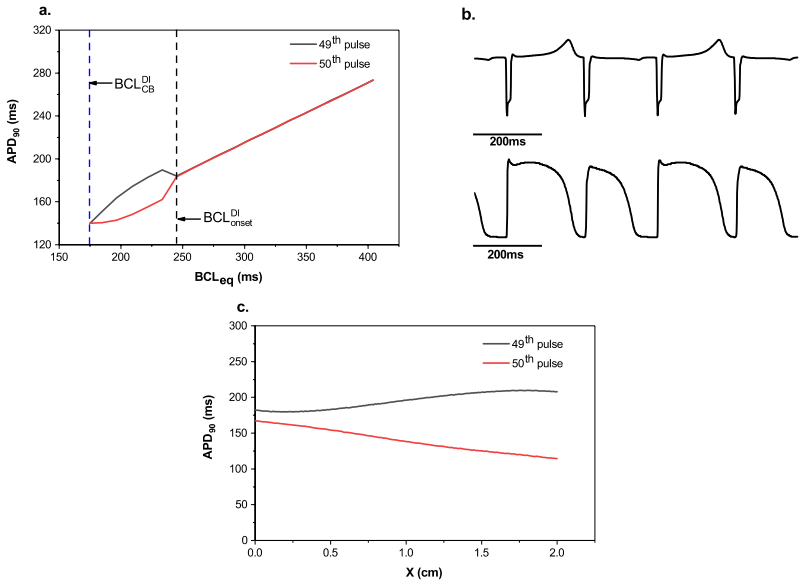

Figure 2.3: 1D human ventricular cable (L = 2 cm) paced using constant DI protocol. (a) Bifurcation diagram at x=0.5 cm; CB at BCL_{CB}^{DI} *= 175 ms is marked with the blue vertical dashed line; onset of alternans at* BCL_{onset}^{DI} *= 245 ms is marked with the black vertical dashed line. (b) A representative pseudo-ECG trace along with corresponding action potential trace of alternans occurring in the cable at* BCL_{eq} *= 209 ms. (c) Steady state* APD_{90} *values along a 2 cm cable for the last two stimuli pulses (49th and 50th) at a* BCL_{eq} *= 209 ms demonstrating SCA alternans.*

SDA alternans were observed when a longer (for instance, L=5 cm) cable was paced under both constant TR and constant DI pacing protocols at a smaller BCL = 253 ms, as indicated in Fig. 2.5. Under constant TR pacing (Fig. 2.5(a)), two intersection points or nodal points were observed, across which the alternans pattern changed its phase. In the case of constant DI pacing (Fig. 2.5(b)), only one nodal point was observed.

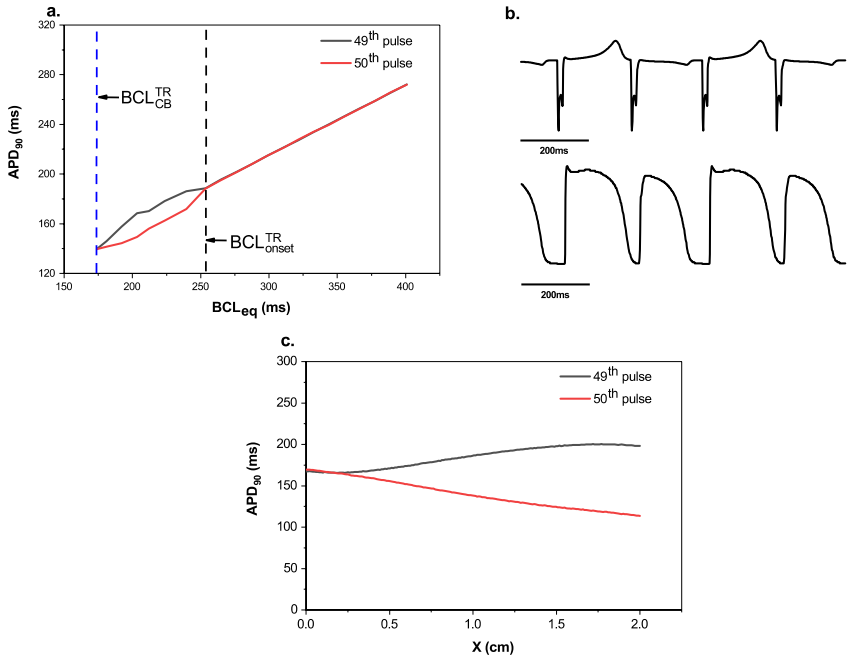

Figure 2.4: 1D human ventricular cable (L = 2 cm) paced using constant TR pacing. (a) Bifurcation diagram at x=0.5 cm; CB at BCL_{CB}^{TR} = 174 ms is marked with the blue vertical dashed line; onset of alternans at BCL_{onset}^{TR} = 253.5 ms is marked with the black vertical dashed line. (b) A representative pseudo-ECG trace along with corresponding action potential trace of alternans occurring in the cable at BCL_{eq} = 212 ms. (c) Steady state APD_{90} values along a 2 cm cable for the last two stimuli pulses (49_{th} and 50_{th}) at a BCL_{eq} = 212 ms demonstrating SCA alternans.

2.3.2 Dynamic responses of ventricular fiber to constant DI and constant TR pacing

Different dynamical responses, specifically 1:1 response, SCA, SDA, and CB, were classified and are shown in Fig. 2.6(a), (b) for both constant DI and constant TR pacing, respectively, for different L. Figure 2.6 also includes the onset of alternans that occurs during periodic pacing, BCL_{onset}^{BCL} = 346 ms (black vertical dashed line), for comparison purposes [11]. Our results indicate that both constant TR and constant DI pacing protocols are superior to constant BCL pacing in preventing the onset of alternans until smaller BCLs. However, constant TR pacing and constant DI pacing resulted in different dynamical responses of the cardiac myocytes for all L > 1 cm. Specifically, for L = 2 cm and L= 3 cm, constant DI pacing prevented the onset of alternans better than constant TR pacing. For L = 4 cm, both the protocols exhibited similar performance. Whereas for L > 4 cm, it was observed that both the protocols resulted in SDA alternans at lower BCL, but constant TR pacing showed an improved ability in preventing them.

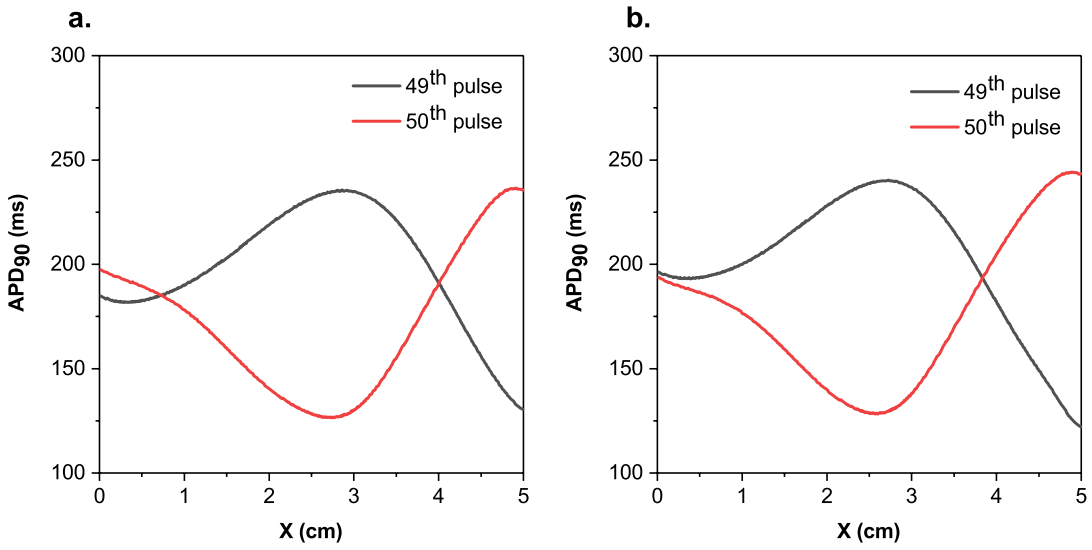

Figure 2.5: Spatially discordant alternans (SDA) in a 1D human ventricular cable (L ==5 cm) that was paced using (a) constant TR and (b) constant DI pacing protocols at BCL_{eq} *=253 ms*

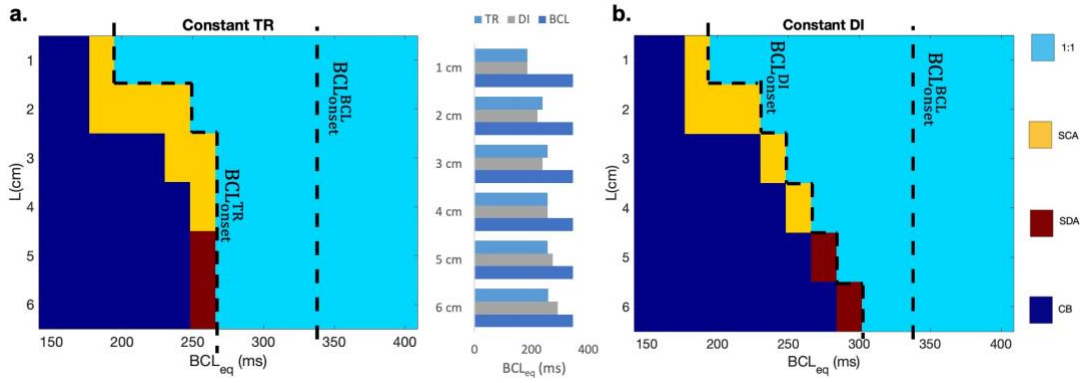

Figure 2.6: Classification of different dynamic responses (1:1, SCA, SDA, and CB) in a1D human ventricular cable of different length L when it was paced at different BCLs using either (a) constant TR and (b) constant DI pacing protocols. The vertical dashed line represents the onset of alternans under constant BCL pacing, showing BCL_{onset}^{BCL} *= 346 ms (see Fig. 4A in [11]).*

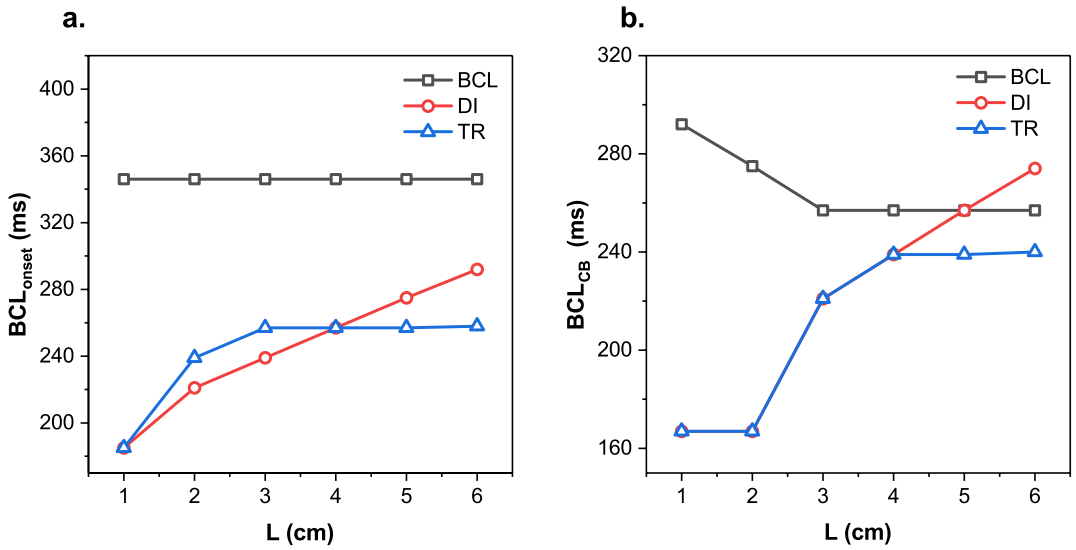

Figure 2.7: (a) BCL_{onset} for constant BCL (black line), constant TR (blue line) and constant DI (red line) pacing protocols as a function of cable length, (b) BCL_{CB} for constant BCL (black line), constant TR (blue line) and constant DI (red line) pacing as a function of cable length L.

In Figure 2.7, BCL_{onset} and BCL_{CB} for both constant TR and constant DI pacing protocols, are plotted as a function of cable length L. From Fig. 2.7(a), it can be seen that BCL_{onset}^{BCL} remains constant irrespective of L. Note that BCL_{onset}^{DI} is gradually increasing as L increases. On the other hand, BCL_{onset}^{TR} is increasing first, and then remains constant (and smaller than BCL_{onset}^{DI}) for L $\geq$ 4 cm. Similarly, BCL_{CB}^{TR} remains constant for L $\geq$ 4 cm while BCL_{CB}^{DI} increases linearly with an increase in L (see Fig. 2.7(b)).

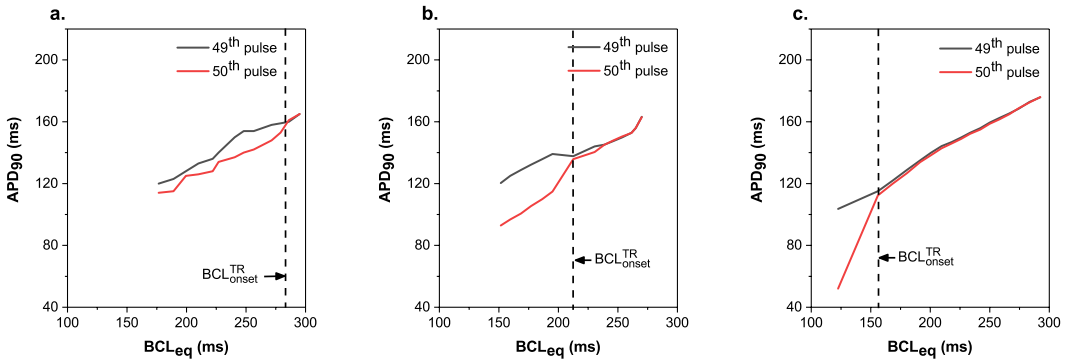

Figure 2.8: APD bifurcation diagrams plotted at x =0.5cm, demonstrating the effectiveness of constant TR pacing protocol in suppressing alternans in a 2 cm ventricular rabbit cable in the case of (a) strong, (b) normal, and (c) weak voltage-calcium coupling strength. An onset of alternans is marked with black vertical dashed line: BCL_{onset}^{TR} = (a) 277 ms, (b) 212 ms, (c) 156 ms.

2.3.3 Response to Constant TR pacing for different voltage-calcium coupling levels

The effectiveness of constant TR pacing for various levels of voltage-calcium coupling was studied in the rabbit ventricular model of L = 2 cm. The effect of g_{NaCa} modulation is illustrated in Fig. 2.8, where APD90 bifurcation diagrams are plotted for strong, normal, and weak voltage-calcium coupling. The onset of alternans (BCL_{onset}^{TR}) was found to be 277 ms, 212 ms, and 156 ms, respectively, for strong, normal, and weak coupling. These values indicate that the performance of constant TR pacing is deteriorated for stronger coupling, while its effectiveness is increased for weaker coupling. Thus, constant TR pacing becomes increasingly more antiarrhythmic for decreasing voltage-calcium coupling.

2.4 Discussion

Suppressing cardiac alternans by applying pacing mechanisms has been widely researched with the goal of reducing the risk of developing arrhythmias. In this study, constant DI and constant TR pacing protocols were employed in a 1D numerical model of a human ventricular cable, and their abilities to prevent the formation of alternans were compared. The major findings of the study are as follows: (1) Both constant TR pacing and constant DI pacing are superior to traditional BCL-based control mechanism, (2) constant TR pacing is more efficient than constant DI pacing preventing alternans for longer cable lengths, and (3) constant TR pacing is more antiarrhythmic for weaker voltage-calcium coupling and its performance deteriorates for strong coupling.

While both the constant DI and constant TR pacing protocols intend to trigger stimulation after a predetermined DI/TR interval after the end of the APD, there is a fundamental difference between the two protocols. The constant DI protocol triggers the stimulus after determining DI from single-cell measurements in the cable, which is similar to microelectrode recording. On the other hand, constant TR protocol takes into account the electrical activity of the entire cable to determine a TR interval to trigger the stimulus. This TR interval represents the "averaged" measure of all DIs along the cable, thus including action potential propagation, as well as possible spatial inhomogeneity, such as dispersion of APD and CV refractoriness. In this study, only action potential propagation was responsible for the differences in the efficacy of the two protocols to prevent alternans formation. Clearly, the shorter the cable, the closer are the determined DI and TR intervals. Our results demonstrate that as the cable length increases, the constant TR pacing results in more anti-arrhythmic than constant DI

pacing. Further studies need to be elucidated to determine the contribution of spatial inhomogeneity to the differences in constant DI and constant TR protocols performances.

Results of this study showed that constant TR and constant DI pacing are much more anti-arrhythmic than a periodic (constant BCL) pacing, since both of them resulted in the formation of alternans at much lower BCL. Both constant DI pacing and constant TR pacing exhibited similar performance in preventing the earlier onset of alternans for L = 1 cm cable. For 1 cm < L < 4 cm, constant DI pacing performed better in preventing earlier onset than constant TR pacing. For longer cable lengths (L > 4 cm), both constant TR and constant DI pacing resulted in SDA alternans for smaller BCLs (higher pacing rates). SDA alternans are more dangerous since they increase the dispersion of refractoriness, which can result in a conduction block and can create a substrate that leads to wave breaks and reentry [36]. Since constant TR pacing prevented the earlier onset of alternans for much longer length cables when compared to constant DI pacing, constant TR pacing exhibited a greater control on alternans.

The underlying interdependency between membrane voltage and intracellular calcium cycling plays an important role in the formation of alternans. It has been shown (Fig. 2.8) that the amount of voltage-calcium coupling impacted the efficacy of constant TR pacing. Weak voltage-calcium coupling in the cellular level favored the constant TR pacing in shifting the BCL_{onset} for alternans to smaller values, while the effectiveness of constant TR pacing significantly reduced under strong voltage-calcium coupling. Similar results for constant DI pacing was demonstrated by Zlochiver et. al. [11], where the increased effectiveness was achieved for decreasing coupling levels.

2.4.1 Study limitations

Our study involves the following limitations. This study used well-established kinetic models that have been widely used and validated [37]. However, this numerical model cannot account for the inherent variability in living tissue. Because of this, an experimental validation of these results should be done. Another important limitation of this study was that the effects of voltage-calcium coupling was not evaluated. The influence of calcium-induced alternans should be evaluated in subsequent work. The effects of varying restitution slope on alternans were also not evaluated in this study, since the focus of the experiment was to compare constant TR and constant DI pacing in suppressing alternans formation so a steep restitution slope of 1.8, which increases the likelihood of alternans, was used. Also, this study only considers homogenous tissue and thus does not take into account the changes in the spatial and temporal evolution of alternans due to different cell types (epi, endo, M, apex-base). The performance of constant DI and constant TR protocols in the presence of tissue in-homogeneity might be different. Furthermore, this study uses a 1D cable for the simulation, which prevents assessing the effect of alternative ECG lead placements on alternans control. Hence, a 2D or 3D tissue simulation needs to be performed to further investigate the efficacy of constant TR pacing under such conditions.

2.4.2 Conclusions

Cardiac alternans are a period-2 rhythm where the APD of cardiac myocytes alternates between long and short values and increase the risk of developing life-threatening arrhythmias. The constant DI pacing has been employed previously in

numerical models and has been successful in suppressing alternans onset to higher pacing rates. The constant TR pacing, a global analogy to constant DI pacing, was studied for the first time using a 1D numerical model of ventricular fiber. Both of these pacing protocols were superior to periodic pacing in preventing alternans onset. Moreover, constant TR pacing was found to be more anti-arrhythmic than constant DI pacing for longer cable lengths and should be further validated in animal experiments.

CHAPTER 3: *VIEgram* FOR ANALYSIS AND VISUALIZATION OF ELECTROGRAMS

(The work in this chapter has been accepted for publication as Sanket Thakare, Siva K. Mulpuru, Henri Roukoz and Elena G. Tolkacheva, "VIEgram – Analysis and Visualization of Intracardiac Electrograms on Patient-Specific 3D Atria Model", IEEE EMBC, 2020)

Author Contributions:

Concept was developed by E.G.T., H.R. and S.T. *VIEgram* software was developed by S.T. Data was analyzed by S.T. and prepared for publication by S.T. and E.G.T.

Abstract

Over the last few years, the use of cardiac mapping for effective diagnosis and treatment of arrhythmias has increased significantly. In the clinical environment, electroanatomical mapping (EAM) is performed during the electrophysiological procedures using proprietary systems such as CARTO, EnSite Precision, RHYTHMIA, etc. These systems generate the 3D model of patient-specific atria with the electrical activity (i.e., intracardiac electrograms (iEGMs)) displayed on it, for further identification of the sources of arrhythmia and for guiding cardiac ablation therapy. Recently, several novel techniques were developed to perform iEGMs analysis to more accurately identify the arrhythmogenic sites. However, there is a difficulty in incorporating the results of iEGMs analysis back to EAM systems due to their proprietary constraints. This created a hurdle in the further development of novel techniques to help navigate patient-specific clinical ablation therapy. Thus, we developed an open source software, *VIEgram*[1], that allows researchers to visualize the results of the various iEGMs analysis on a patient-specific 3D atria model. It eliminates the dependency of the academic environment on the proprietary EAM systems, thereby making the process of retrospective mapping extremely convenient and time efficient. Here, we demonstrate the features of *VIEgram* such as visual inspection of iEGMs, flexibility in implementing custom iEGMs analysis techniques and interpolation schemes, and spatial analysis.

3.1 Introduction

Arrhythmias, which are caused by the irregularities in the electrical activity of the heart, is the number one cause of sudden cardiac death. Atrial fibrillation (AF), the most common sustained arrhythmia, is associated with heart failure, stroke and other heart related complications [38], [39].

In recent years, catheter ablation procedure, in which regions radiating irregular electrical activity is ablated, has become a mainstay of treatment for AF, largely due to the advancements in cardiac mapping technology. Electroanatomical mapping (EAM) is the process of mapping intracardiac electrograms (iEGMs) recorded from endocardial sites during electrophysiological study to the respective spatial sites [40], and it is widely used to guide ablation procedure. In the clinical setting, proprietary EAM systems, such as CARTO, EnSite Precision, RHYTHMIA, etc., are used to visualize the iEGMs on a patient's 3D atria model and to identify the potential target sites for AF ablation.

The availability of iEGM data from EAM systems has allowed researchers to perform offline analysis of iEGMs in academic environment, and to further develop several novel analysis techniques for more accurate identification of target sites for ablation [41]–[44]. To ensure whether the developed technique has a diagnosing capability, the results of the offline analysis has to be properly visualized on a 3D model of patient's atria. To date, the only way to achieve this goal is to manually input the results of analysis into the proprietary EAM systems that are currently used in clinics. However, this step is extremely time-consuming, and it also requires the use of expensive EAM systems outside of their clinical intended purpose. Thus, there is a need

for a software that will allow 3D visualization of the various iEGMs analysis on a patient-specific atria model for all off-site analysis of clinical iEGMs in the academic environment.

Previously, Linton et al. developed a software called Ripple-mapping to visualize the improvised local activation time (LAT) maps [45]. However, the software is only specific to LAT analysis. An open source modular software was developed by Cantwell et al. [46], which allows visualization of a set of pre-defined techniques. Since the software was written in C++, its usage was resisted by researchers as they are used to developing and customizing tools in MATLAB to fit their unique analysis requirements. Recently, Oesterlein et al. developed the visualization software KaPAVIE (Karlsruhe Platform for Analysis and Visualization of Intracardiac Electrograms) [47]. It uses MATLAB for iEGMs analysis, and therefore it is very attractive for research purposes since it allows easy incorporation of the newly developed techniques. However, one of the limitations of the KaPAVIE software is the use of fixed interpolation scheme irrespective of the nature of iEGMs dataset. Indeed, acquired clinical data can be sparse or dense depending on the EAM system used, and the use of the same interpolation scheme may mislead the interpretation of the results, and therefore it further restrains the user from performing localized spatial analysis. Also, KaPAVIE runs on MacOS and not all researchers work on MacOS, thus restricting those researchers from using it for analysis and visualization of iEGMs.

Here, we present our recently developed open-source software called *VIEgram* to support the analysis of iEGMs and to perform 3D visualization of the analysis results. *VIEgram* integrates the data handling capabilities of Python and powerful algorithm

development environment of MATLAB. We present the performance of *VIEgram* using a set of clinically recorded iEGMs from a patient with persistent AF. We believe that *VIEgram* will further facilitate the development of novel iEGMs analysis techniques.

3.2 Methods

3.2.1 Clinical Data Collection and Analysis

The clinical iEGMs were collected from a patient with persistent AF during an EP study at the Mayo clinic (Rochester, MN), with prior approval under institutional review board approved protocol. Informed consent was obtained from the patient with persistent AF.

EAM was performed using the CARTO (Biosense Webster, CA, USA) system. The CARTO mapping system has a sensor position accuracy of 0.8 mm and 5°. High resolution PentaRay NAV catheter (Biosense Webster, CA) was used in a sequential scanning approach to fully map both atrial chambers. The 3D geometry of the chamber was reconstructed in real time, and at each point, the system records the unipolar and bipolar iEGMs, sampled at 977 Hz thus allowing the electrophysiological information to be color coded and superimposed on the anatomic map. Ten bipolar electrograms were recorded at each spatial site.

The data were exported from the CARTO system in .txt format, containing 2.5 s iEGMs. A total of 1055 iEGMs were obtained from the patient with 642 iEGMs in the left atrium (LA) and 413 iEGMs in the right atrium (RA). The geometries of LA and RA were obtained in the form of triangulated surface meshes. The exported data also contained the catheter coordinates, i.e. the spatial locations from which the iEGMs

were obtained. The iEGMs with high noise corruption and loss of contact while recording was removed from future analysis. The rest of the clean iEGMs were filtered by a digital bandpass filter of 3-30Hz to limit the frequencies to physiological ranges.

3.2.2 Software Description

i. Overview

VIEgram was primarily developed using Python (3.7.0) and MATLAB (R2018a), which are easily available in all major operating systems (OS) including Windows and MacOS, thus eliminating OS-dependency of our software. The overview of *VIEgram* is shown in Fig. 3.1, where academic setting refers to the off-site for analyzing the data collected from EAM systems used in clinics. A custom-built Python script was used for data extraction, while data processing and 3D mapping was done using custom-built MATLAB script. MATLAB App Designer was used to develop the user interface of the *VIEgram* (See Fig. 3.2).

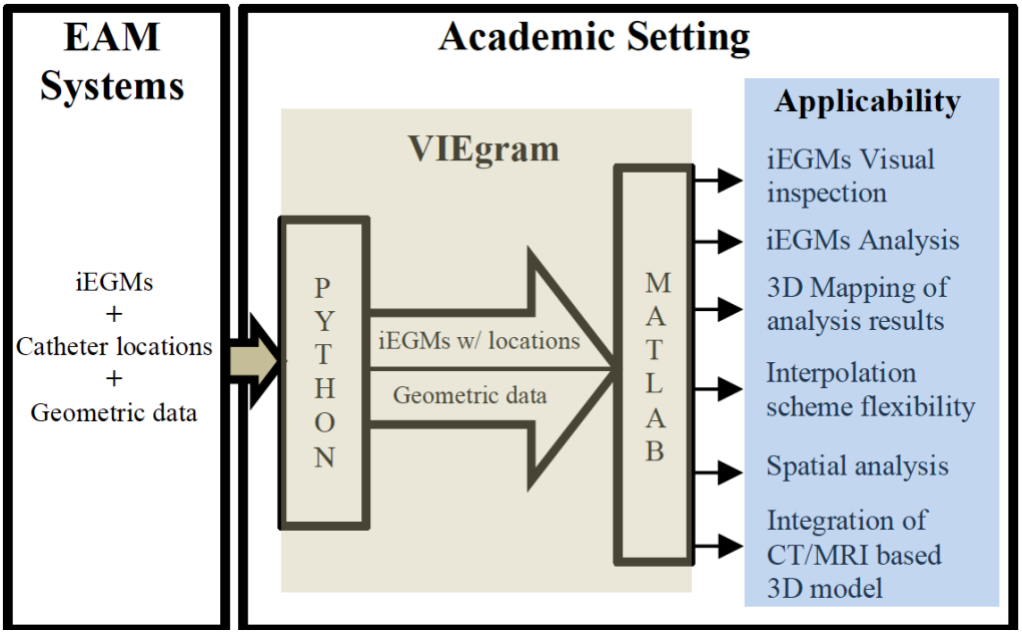

Figure 3.1: Overview of the open-source software VIEgram

ii. Python Script

The typical exported data from EAM system is a mix of iEGMs, catheter locations and geometric data. After studying the format and pattern of the names of files generated by CARTO, Python script was developed to extract these different types of data separately. This script allows to choose either LA and/or RA for analysis and the type of iEGMs – unipolar or bipolar. This flexibility allows for separate implementation of the analysis techniques for bipolar and unipolar data. iEGMs and geometric data extracted using Python script serves as an input to the MATLAB script.

iii. MATLAB Script

The MATLAB script was developed to implement different iEGM analysis techniques and to map the results of these techniques on a 3D atria model. As an example, for this manuscript, we implemented multiscale entropy (MSE) [43] and multiscale frequency (MSF) [41] as iEGMs analysis techniques to demonstrate the capability of *VIEgram*. One of the advantages of the MATLAB script is the potential to easily incorporate and perform 3D visualizations of *various* analysis techniques, per researcher's choice.

iv. Interpolation

For generating 3D maps, a commonly used interpolation scheme called nearest neighbor interpolation was used as a default setting. It is implemented using the following equation:

$$Zp = \frac{\sum_{i=1}^{n}\left(\frac{Zi}{di^m}\right)}{\sum_{i=1}^{n}\frac{1}{di^m}} \quad (1)$$

where *Zp* is the estimation at point *p*, *Zi* is the value at point *i*, *di* is the distance between point *i* and point *p*, and *m* is the power parameter. However, the MATLAB script provides the flexibility of implementing *custom interpolation* schemes for better visualization of 3D results.

3.3 Results

3.3.1 VIEgram User Interface

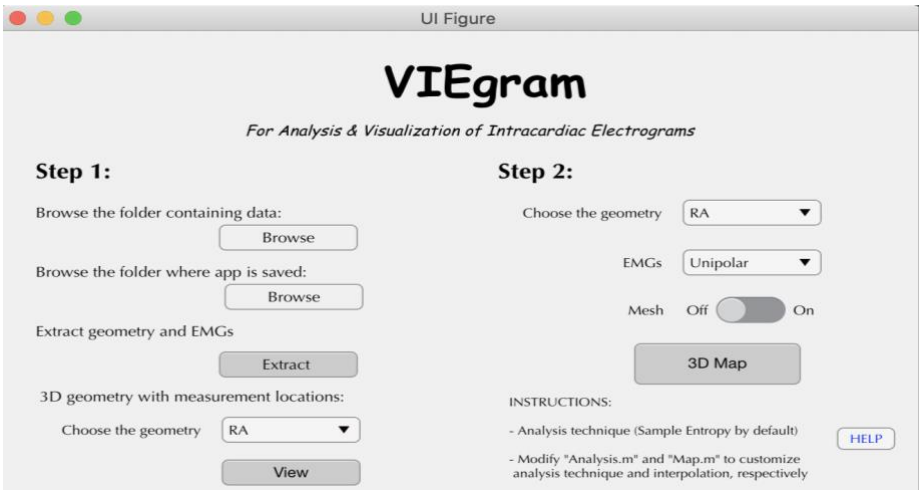

Figure 3.2: User interface of VIEgram software to extract and analyse iEGMs, and to visualize the results on 3D atria model.

Fig. 3.2 shows the user interface of the *VIEgram.* In Step 1, user will be able to extract geometry data of atria and recorded unipolar and bipolar iEGMs with their corresponding locations from EAM systems. Currently, *VIEgram* is compatible with CARTO EAM system, but in the future, extraction modules for other EAM systems can be developed. Extracted data are saved in the "Data" folder of the *VIEgram* in the csv format. User can also visualize the geometry with the locations of recorded iEGMs highlighted (see Fig. 3.3 top panel). In Step 2, analysis of iEGMs is performed (for

instance using MSE and MSF), and the results of the analysis is visualized on the 3D geometry of heart. The software includes two user-access files, “Analysis.m” and “Map.m”, which can be modified to add additional iEGMs analysis techniques, and to implement different interpolation schemes, respectively.

3.3.2 Patient-Specific 3D Atria Model

Fig. 3.3 shows the 3D geometrical model of RA (dark grey) and LA (light grey) of the AF patient generated by *VIEgram* based on geometrical data from the CARTO system. The green dots indicate the sites at which iEGMs were recorded. Note that the spatial distribution of the iEGMs is very sparse, and therefore the importance of adequately choosing the interpolation technique and its parameters.

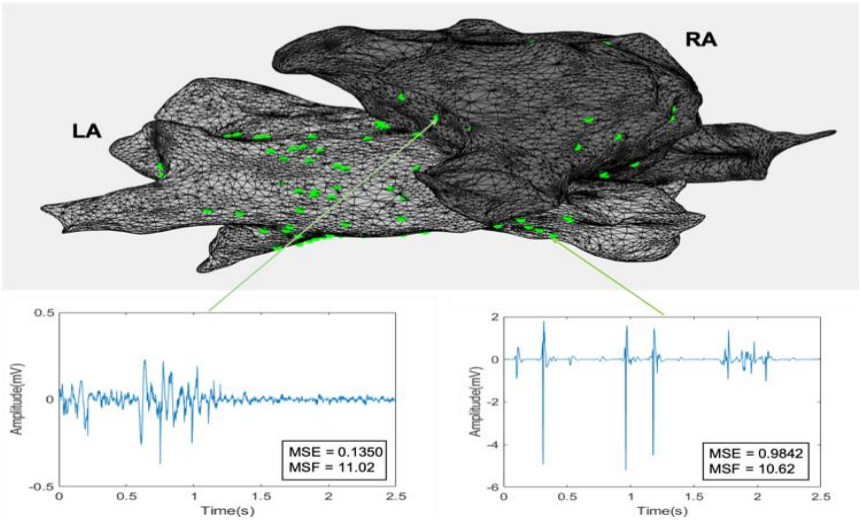

Figure 3.3: Top panel shows the patient-specific 3D atria model, with LA (light grey) and RA (dark grey). Green dots indicate the location of clinically recorded iEGMs, which examples are shown on the bottom.

3.3.3 3D Maps

For testing the *VIEgram* software, MSE and MSF analysis of bipolar iEGMs from both RA and LA were implemented and further visualized (see Figs. 3.4 and 3.5, respectively). Spatial sites having greater value, i.e. the brighter color regions, indicate the presence of potential AF active sites. We can see from Figs. 3.4 and 3.5 that estimated potential active AF sites appeared to be outside the PV regions for both MSE and MSF analysis, which is consistent with the current hypothesis [48] for maintaining AF in the case of persistent AF.

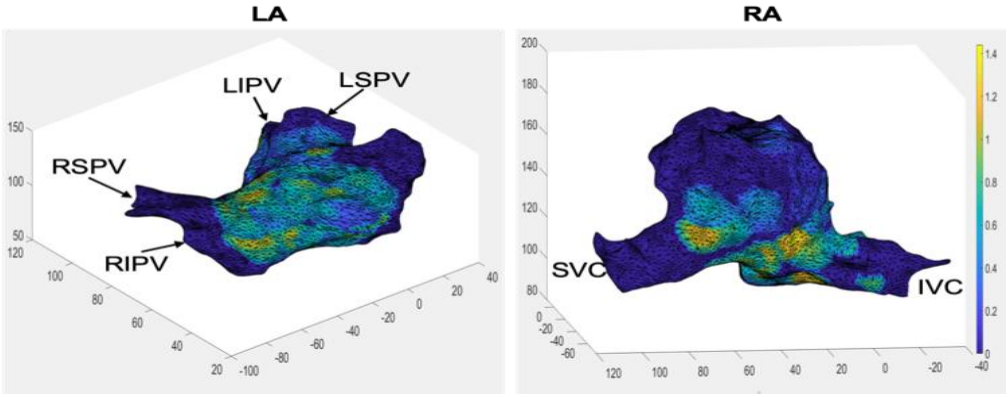

Figure 3.4: 3D visualization of the MSE analysis on the LA (left panel) and RA (right panel). Several anatomical hallmarks are shown: LSPV – Left Superior Pulmonary Vein (PV), LIPV – Left Inferior PV, RSPV – Left Superior PV, RIPV – Left Inferior PV, RSPV – Left Superior PV, RIPV – Left Inferior PV, SVC – Superior Vena Cava, IVC – Inferior Vena Cava.

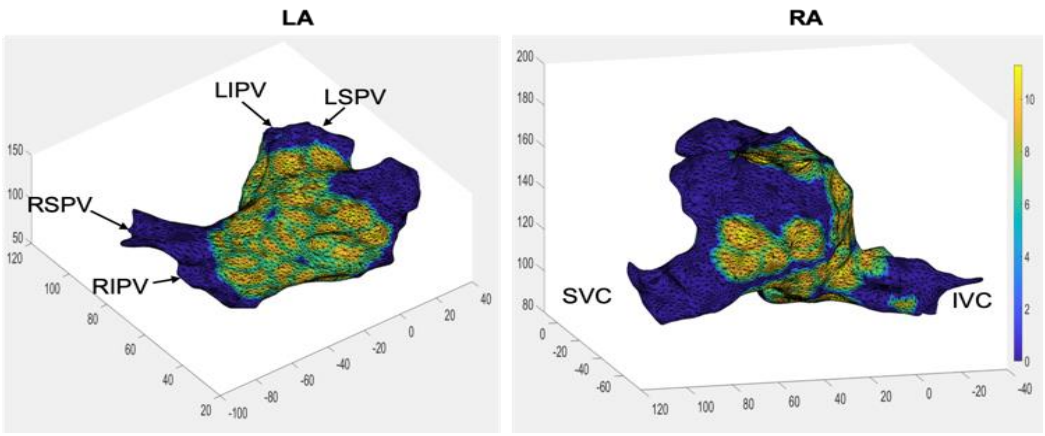

Figure 3.5: 3D visualization of the MSF analysis on the LA (left panel) and RA (right panel).

3.3.4 Customizable Interpolation

For interpolation, nearest neighbor interpolation with power parameter, m=1, was implemented as a default scheme (see Fig. 3.6, left panel). To show the flexibility in modifying or implementing a custom interpolation scheme, nearest neighbor interpolation with m=4 was implemented (see Fig. 3.6, right panel).

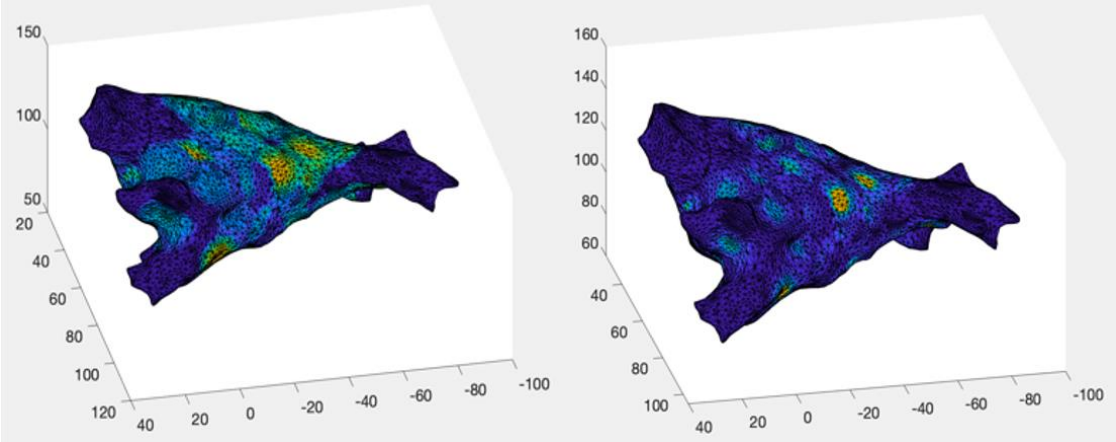

Figure 3.6: 3D visualization of the MSE analysis using nearest neighbor interpolation scheme (see Eq. (1)) with different power parameter : m=1 (left panel) and m=4 (right panel).

A significant difference can be noticed between MSE 3D maps with different interpolation. Thus, the choice of interpolation scheme plays a major role in representing the results of analysis.

3.3.5 Spatial Analysis of iEGMs

VIEgram allows to perform spatial analysis of iEGMs. To demonstrate this, LA was divided to 10 different spatial regions (see Fig. 3.7): LA appendage, lateral wall, roof wall, posterior wall, inferior wall, septal wall, left superior PV (LSPV), left inferior PV (LIPV), right superior PV (RSPV) and right inferior PV (RIPV). Region growing algorithm using face distance (distance between face vertices) was used to segment different spatial regions. The seed face was manually chosen for each of those 10 spatial regions in LA. The left panel in the Fig. 3.7 shows the location of these regions from different perspectives. The right panel in Fig. 3.7 shows the projection of multi-spline catheter mapped on to these regions where black dots indicate the recording sites. This allows the researcher to perform spatial analysis and correlate the performance between different catheters. In addition, *VIEgram* allows to enable (left panel) or disable (right panel) the mesh structure for better visualization.

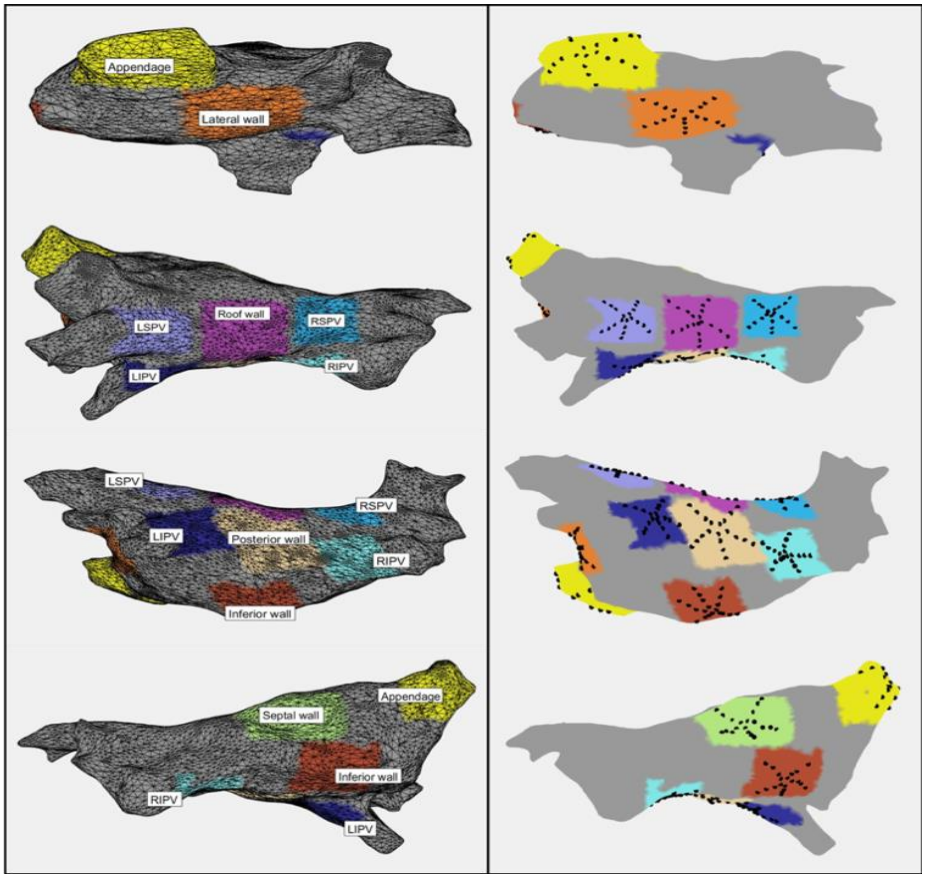

Figure 3.7: Ten different regions of LA with a mesh structure (left panel) and projection of multi-spline catheter mapped to each of these regions without a mesh structure (right panel).

3.4 Discussion

In this work, we developed *VIEgram*, a MATLAB based software, to analyze and visualize the results of iEGMs analysis on a 3D atria model. The use of MATLAB in developing *VIEgram* enables the researchers to easily modify the script, which makes it more customizable for both analysis and visualization. This allows to do the required modifications to suit the acquired iEGM dataset and type of analysis. *VIEgram* was demonstrated to perform custom actions such as 1) visual inspection of iEGMs, 2)

implement custom iEGMs analysis techniques, 3) mapping analysis results on a patient-specific 3D atrium with customizable interpolation scheme, and 4) spatial analysis of iEGMs. These capabilities make the process of retrospective mapping extremely convenient for academic researchers. Currently, *VIEgram* is compatible with the CARTO system, but in the future, additional compatibility with other EAM systems can be easily incorporated by developing the supporting modules.

Previously, several software applications were developed to visualize the results of iEGMs analysis on a patient-specific 3D atria model [45]–[47]. However, they have multiple limitations:1) no provision for implementing custom analysis techniques,2) C++ based development environment which makes it difficult for academic researchers to implement their MATLAB developed analysis techniques, 3) operating system dependency, and 4) no control over visualization which precludes the researchers from implementing different interpolation schemes and spatial analysis.

Quantitative evaluation of arrhythmic sites and the utilization of various diagnostic methodologies have become more widely used in clinics. However, one potential problem is that some methods are covered with insurance and some not, thus providing additional burden on clinicians. In addition, the insurance coverage associated with the use of various diagnostic methodologies can be problematic in developing countries. 3D models from *VIEgram* can be further integrated with the CT/MRI based 3D models to incorporate fibrosis and scar data. Therefore, *VIEgram* can provide an additional support in integrating the results of different cardiac imaging modalities with 3D visualizations for better identification of AF ablation sites. In the future, *VIEgram*

will equip not only the researchers but also the clinicians with a tool to study, analyze, and visualize iEGMs.

3.5 Conclusion

We developed new software, *VIEgram*, for the analysis and visualization of iEGMs. This software allows researchers to use clinical data from EAM systems to study the iEGM morphology, implement their own iEGMs analysis techniques, generate 3D maps corresponding to those techniques, perform region specific localized analysis, and integrate the generated 3D models with the 3D models generated using CT/MRI scan data to incorporate anatomical and functional information of heart. Altogether, *VIEgram* equips the researcher with a tool to study, analyze and visualize iEGMs, thus providing a testing and validation capability prior to clinical implementation.

CHAPTER 4: CONCLUSIONS AND FUTURE RECOMMENDATIONS

The thesis targeted different aspects of cardiac arrhythmias. One of the aims was to assess the efficacy of clinically feasible, ECG-based constant TR pacing to control the proarrhythmic alternans, while the second was to develop visualization software to facilitate the development and validation of novel iEGMs analysis techniques to detect the target sites for ablation to treat the most common arrhythmia, atrial fibrillation. The aims were achieved using the principles of non-linear cardiac dynamics and the fundamentals of cardiac anatomy and electrophysiology.

The main conclusions of this research are:

1. Constant TR pacing, a clinically feasible pacing protocol, is more anti-arrhythmic in 1D ventricular cable model than the periodic pacing, an approach used by most of the contemporary cardiac pacemakers.
2. Constant TR pacing was found to be more beneficial in preventing alternans than constant DI pacing in the ventricular cables of longer lengths.
3. *VIEgram*, an analysis and 3D visualization software, demonstrated the well-needed flexibility in implementing user-defined iEGMs analysis techniques as well as in visualizing the analysis results on a patient's 3D atria model, thereby providing a testing capability before clinical implementation.

4.1 Clinical translation of Constant TR pacing

Constant TR pacing was implemented in a 1D numerical model of homogeneous human ventricular tissue where onset of alternans was used as an indication of the stability by investigating its propensity to transition into abnormal rhythms. Though the results show constant TR pacing as more anti-arrhythmic than constant DI pacing, the 1D numerical model does not take into account the inherent in-homogeneities, and the spatial and temporal evolution of alternans. Thus, constant TR pacing needs to be implemented in 2D or 3D numerical models to study its efficacy in controlling alternans. The next step then would be to implement constant TR pacing on ex-vivo isolated whole hearts to validate its beneficial anti-arrhythmic effects. Later, it can be preclinically adapted in the prototype pacemaker to perform in-vivo experiments in swine models which will further lay the foundation for smoother adaptability into future human trials.

4.2 Future scope of VIEgram

Catheter ablation procedure has been widely used to treat AF, the most common arrhythmia and a major contributor to morbidity and mortality. The standard-approach is pulmonary vein isolation (PVI), which encircles the pulmonary veins with lesions, preventing abnormal electric signals generated in the veins [39]. All the attempts to target the arrhythmogenic sources like linear ablation lesions across the left atrial roof and mitral valve isthmus, and ablations of complex fractionated atrial electrograms (CFAE), have failed to deliver reasonable outcomes further leading to multiple failed ablations [49]. This led to the development of several novel analysis approaches in automating the estimation of the potential target sites for ablation. However, hardly any

of these approaches have translated for clinical utility due to the lack of a visualization tool to perform retrospective mapping of the analysis results on the patient's 3D heart model and the subsequent clinical discussion to ensure its clinical feasibility. *VIEgram* with few upgrades can be a tool that can potentially be used to facilitate the translation of these novel approaches in the clinical setting for the ablation procedure.

The novel analysis approaches that have been developed are based on different principles. Some approaches try to detect the abnormal spectral changes (eg. dominant frequency, multiscale frequency [50]), some try to measure the uncertainty (eg. sample entropy, multiscale entropy [50]), while some are statistical-based (eg. kurtosis [50]). Correlation analysis between these different analysis techniques can help identify the precise location of target sites to guide catheter ablation. Such a provision in *VIEgram* can help to visualize the sites that show a strong correlation, thereby providing a robust estimate of potential AF ablation sites in a patient-specific manner. Also, the correlation analysis of newly developed approaches with the clinically used approaches like local activation time maps (LAT), CFAE, and phase mapping can provide insights into the organization and location of AF maintaining substrates.

The patients with the persistent form of AF typically develop a fibrotic remodeling in the atria [51]–[54]. The developed fibrotic substrate then perpetuates the re-circulating electrical waves [55] thereby becoming an AF sustaining substrate. The non-invasive late gadolinium enhancement magnetic resonance imaging (LGE-MRI) helps to delineate the locations of the fibrotic substrate. Thus, an additional feature in *VIEgram* to integrate the analysis mapped 3D model with the LGE-MRI based 3D

model will help to predict the ablation targets in the fibrotic substrate. This will further help to customize the ablation targets for each patient.

REFERENCES

[1] Z. Qu, G. Hu, A. Garfinkel, and J. N. Weiss, “Nonlinear and stochastic dynamics in the heart,” *Phys. Rep.*, vol. 543, no. 2, pp. 61–162, 2014, doi: 10.1016/j.physrep.2014.05.002.

[2] J. N. Weiss *et al.*, “Perspective: A dynamics-based classification of ventricular arrhythmias,” *J. Mol. Cell. Cardiol.*, vol. 82, no. 2015, pp. 136–152, 2015, doi: 10.1016/j.yjmcc.2015.02.017.

[3] J. M. Pastore, S. D. Girouard, K. R. Laurita, F. G. Akar, and D. S. Rosenbaum, “Mechanism linking T-wave alternans to the genesis of cardiac fibrillation,” *Circulation*, vol. 99, no. 10, pp. 1385–1394, 1999, doi: 10.1161/01.CIR.99.10.1385.

[4] J. J. Fox, J. L. McHarg, and R. F. Gilmour, “Ionic mechanism of electrical alternans,” *Am. J. Physiol. - Hear. Circ. Physiol.*, vol. 282, no. 2 51-2, pp. 516–530, 2002, doi: 10.1152/ajpheart.00612.2001.

[5] R. F. Gilmour, “Electrical Restitution and Ventricular Fibrillation: Negotiating a Slippery Slope,” *J. Cardiovasc. Electrophysiol.*, vol. 13, no. 11, pp. 1150–1151, doi: 10.1046/j.1540-8167.2002.01150.x.

[6] A. Karma, “Electrical alternans and spiral wave breakup in cardiac tissue,” *Chaos*, vol. 4, no. 3, pp. 461–472, 1994, doi: 10.1063/1.166024.

[7] M. Watanabe, N. F. Otani, and R. F. Gilmour, “Biphasic restitution of action potential duration and complex dynamics in ventricular myocardium,” *Circ. Res.*, vol. 76, no. 5, pp. 915–921, 1995, doi: 10.1161/01.RES.76.5.915.

[8] L. Escobar and H. Valdivia, “Cardiac Alternans and Ventricular Fibrillation: A Bad Case of Ryanodine Receptors Reneging on Their Duty,” *Circ. Res.*, vol. 114, no. 9, pp. 1369–1371, doi: 10.1161/CIRCRESAHA.114.303823.

[9] W. Rappel, F. Fenton, and A. Karma, “Spatiotemporal control of wave instabilities in cardiac tissue,” *Phys. Rev. Lett.*, vol. 83, no. 2, pp. 456–459, doi: 10.1103/PhysRevLett.83.456.

[10] E. Tolkacheva, M. Romeo, M. Guerraty, and D. Gauthier, “Condition for alternans and its control in a two-dimensional mapping model of paced cardiac dynamics,” *Phys. Rev. E*, vol. 69, no. 3, p. 031904, doi: 10.1103/PhysRevE.69.031904.

[11] S. Zlochiver, C. Johnson, and E. G. Tolkacheva, “Constant DI pacing suppresses cardiac alternans formation in numerical cable models,” *Chaos An Interdiscip. J. Nonlinear Sci.*, vol. 27, no. 9, p. 093903, doi: 10.1063/1.4999355.

[12] K. Kulkarni, S. Lee, R. Kluck, and E. Tolkacheva, “Real-Time Closed Loop Diastolic Interval Control Prevents Cardiac Alternans in Isolated Whole Rabbit Hearts,” *Ann. Biomed. Eng.*, vol. 46, no. 4, pp. 555–566, doi: 10.1007/s10439-018-1981-2.

[13] N. Ganesan *et al.*, “Bipolar Electrogram Shannon Entropy at Sites of Rotational Activation: Implications for Ablation of Atrial Fibrillation,” *Circ. Arrhythmia Electrophysiol.*, vol. 6, no. 1, pp. 48–57, doi: 10.1161/CIRCEP.112.976654.

[14] M. J. Cutler and D. S. Rosenbaum, “Explaining the clinical manifestations of T wave alternans in patients at risk for sudden cardiac death,” *Hear. Rhythm*, vol. 6, no. 3, pp. S22–S28, 2009, doi: 10.1016/j.hrthm.2008.10.007.

[15] M. Watanabe, N. F. Otani, and J. Gilmour, “Biphasic Restitution of Action Potential Duration and Complex Dynamics in Ventricular Myocardium,” *Circ. Res.*, vol. 76, no. 5, pp. 915–921, doi: 10.1161/01.RES.76.5.915.

[16] S. M. Narayan, “T-Wave Alternans and the Susceptibility to Ventricular Arrhythmias,” *J. Am. Coll. Cardiol.*, vol. 47, no. 2, pp. 269–281, doi: 10.1016/j.jacc.2005.08.066.

[17] E. M. Cherry, “Distinguishing mechanisms for alternans in cardiac cells using constant-diastolic-interval pacing,” *Chaos An Interdiscip. J. Nonlinear Sci.*, vol. 27, no. 9, p. 093902, doi: 10.1063/1.4999354.

[18] S. D. Mcintyre, V. Kakade, Y. Mori, and E. G. Tolkacheva, “Heart rate variability and alternans formation in the heart: The role of feedback in cardiac dynamics,” *J. Theor. Biol.*, vol. 350, pp. 90–97, doi: 10.1016/j.jtbi.2014.02.015.

[19] A. Garzón, R. O. Grigoriev, and F. H. Fenton, “Model-based control of cardiac alternans in Purkinje fibers,” *Phys. Rev. E - Stat. Nonlinear, Soft Matter Phys.*, vol. 84, no. 4, p. 041927, doi: 10.1103/PhysRevE.84.041927.

[20] P. Jordan and D. Christini, “Adaptive diastolic interval control of cardiac action potential duration alternans,” *J. Cardiovasc. Electrophysiol.*, vol. 15, no. 10, pp. 1177–1185, doi: 10.1046/j.1540-8167.2004.04098.x.

[21] N. F. Otani, “Theory of the development of alternans in the heart during controlled diastolic interval pacing,” *Chaos An Interdiscip. J. Nonlinear Sci.*, vol. 27, no. 9, p. 093935, doi: 10.1063/1.5003250.

[22] B. Echebarria and A. Karma, “Spatiotemporal control of cardiac alternans,” *Chaos An Interdiscip. J. Nonlinear Sci.*, vol. 12, no. 3, pp. 923–930, doi:

10.1063/1.1501544.

[23] G. M. Hall and D. J. Gauthier, “Experimental control of cardiac muscle alternans,” *Phys. Rev. Lett.*, vol. 88, no. 19, p. 198102, doi: 10.1103/PhysRevLett.88.198102.

[24] U. B. Kanu, S. Iravanian, R. F. Gilmour, and D. J. Christini, “Control of Action Potential Duration Alternans in Canine Cardiac Ventricular Tissue,” *IEEE Trans. Biomed. Eng.*, vol. 58, no. 4, pp. 894–904, doi: 10.1109/TBME.2010.2089984.

[25] J. Pinnell, S. Turner, and S. Howell, “Cardiac muscle physiology,” *Contin. Educ. Anaesth. Crit. Care Pain*, vol. 7, no. 3, pp. 85–88, doi: 10.1093/bjaceaccp/mkm013.

[26] M. R. Guevara, G. Ward, A. Shrier, and L. Glass, “Electrical Alternans and Period-Doubling Bifurcations.,” *Comput. Cardiol.*, pp. 167–170, 1984.

[27] S. Dubljevic, S.-F. Lin, and P. D. Christofides, “Studies on feedback control of cardiac alternans,” *Comput. Chem. Eng.*, vol. 32, no. 9, pp. 2086–2098, 2008, doi: 10.1016/j.compchemeng.2007.10.019.

[28] A. Garzón, R. O. Grigoriev, and F. H. Fenton, “Continuous-time control of alternans in long Purkinje fibers,” *Chaos An Interdiscip. J. Nonlinear Sci.*, vol. 24, no. 3, p. 033124, doi: 10.1063/1.4893295.

[29] A. Garzón, R. O. Grigoriev, and F. H. Fenton, “Model-based control of cardiac alternans on a ring,” *Phys. Rev. E. Stat. Nonlin. Soft Matter Phys.*, vol. 80, no. 2 Pt 1, p. 021932, doi: 10.1103/PhysRevE.80.021932.

[30] C. M. Berger, J. W. Cain, J. E. S. Socolar, and D. J. Gauthier, “Control of

electrical alternans in simulations of paced myocardium using extended time-delay autosynchronization," *Phys. Rev. E. Stat. Nonlin. Soft Matter Phys.*, vol. 76, no. 4 Pt 1, p. 041917, doi: 10.1103/PhysRevE.76.041917.

[31] D. J. Christini, M. L. Riccio, C. A. Culianu, J. J. Fox, A. Karma, and R. F. Gilmour, "Control of electrical alternans in canine cardiac purkinje fibers," *Phys. Rev. Lett.*, vol. 96, no. 10, p. 104101, doi: 10.1103/PhysRevLett.96.104101.

[32] D. Zhou *et al.*, "In Vivo and In Silico Investigation Into Mechanisms of Frequency Dependence of Repolarization Alternans in Human Ventricular Cardiomyocytes," *Circ. Res.*, vol. 118, no. 2, pp. 266–278, doi: 10.1161/CIRCRESAHA.115.307836.

[33] C. Omichi *et al.*, "Intracellular Ca dynamics in ventricular fibrillation," *Am. J. Physiol. Heart Circ. Physiol.*, vol. 286, no. 5, p. H1836, doi: 10.1152/ajpheart.00123.2003.

[34] H. Sedghamiz, "An online algorithm for R, S and T wave detection," 2013. https://www.researchgate.net/publication/316960619_An_online_algorithm_for_R_S_and_T_wave_detection.

[35] A. Mahajan *et al.*, "A Rabbit Ventricular Action Potential Model Replicating Cardiac Dynamics at Rapid Heart Rates," *Biophys. J.*, vol. 94, no. 2, pp. 392–410, 2008, doi: 10.1529/biophysj.106.98160.

[36] S. H. Weinberg and L. Tung, "Oscillation in Cycle Length Induces Transient Discordant and Steady-State Concordant Alternans in the Heart (Cycle Length Oscillation in the Heart)," *PLoS One*, vol. 7, no. 7, p. e40477, doi:

10.1371/journal.pone.0040477.

[37] A. Panfilov, “Alternans and spiral breakup in a human ventricular tissue model,” *Am. J. Physiol.*, vol. 291, no. 3, p. 36, doi: 10.1152/ajpheart.00109.2006.

[38] A. S. Go *et al.*, “Prevalence of Diagnosed Atrial Fibrillation in Adults,” *Jama*, vol. 285, no. 18, p. 2370, 2001, doi: 10.1001/jama.285.18.2370.

[39] H. Calkins *et al.*, “2017 HRS/EHRA/ECAS/APHRS/SOLAECE expert consensus statement on catheter and surgical ablation of atrial fibrillation,” *Hear. Rhythm*, vol. 14, no. 10, pp. e275–e444, 2017, doi: 10.1016/j.hrthm.2017.05.012.

[40] R. O. ZF, Issa ZF ; JM, Miller ; DP, Zipes ; Bonow, *Clinical Arrhythmology and Electrophysiology. A Companion to Braunwald’s Heart Disease*. Philadelphia: Elsevier Science, 2009.

[41] S. P. Arunachalam, E. M. Annoni, S. K. Mulpuru, P. A. Friedman, and E. G. Tolkacheva, “Novel multiscale frequency approach to identify the pivot point of the rotor,” *J. Med. Devices, Trans. ASME*, vol. 10, no. 2, pp. 2–3, 2016, doi: 10.1115/1.4033148.

[42] E. M. Annoni, S. P. Arunachalam, S. Kapa, S. K. Mulpuru, P. A. Friedman, and E. G. Tolkacheva, “Novel quantitative analytical approaches for rotor identification and associated implications for mapping,” *IEEE Trans. Biomed. Eng.*, vol. 65, no. 2, pp. 273–281, 2018, doi: 10.1109/TBME.2017.2763460.

[43] A. SP, K. S, M. SK, F. PA, and T. EG, “Novel approaches for quantitative electrogram analysis for intraprocedural guidance for catheter ablation: A case

of a patient with persistent atrial fibrillation," *Nucl. Med. Biomed. Imaging*, vol. 2, no. 2, pp. 1–8, 2017, doi: 10.15761/nmbi.1000121.

[44] S. M. Narayan, D. E. Krummen, K. Shivkumar, P. Clopton, W. J. Rappel, and J. M. Miller, "Treatment of atrial fibrillation by the ablation of localized sources: CONFIRM (Conventional Ablation for Atrial Fibrillation with or Without Focal Impulse and Rotor Modulation) trial," *J. Am. Coll. Cardiol.*, vol. 60, no. 7, pp. 628–636, 2012, doi: 10.1016/j.jacc.2012.05.022.

[45] S. Jamil-Copley *et al.*, "Application of ripple mapping with an electroanatomic mapping system for diagnosis of atrial tachycardias," *J. Cardiovasc. Electrophysiol.*, vol. 24, no. 12, pp. 1361–1369, 2013, doi: 10.1111/jce.12259.

[46] C. D. Cantwell, C. H. Roney, R. L. Ali, N. A. Qureshi, P. B. Lim, and N. S. Peters, "A software platform for the comparative analysis of electroanatomic and imaging data including conduction velocity mapping," *2014 36th Annu. Int. Conf. IEEE Eng. Med. Biol. Soc. EMBC 2014*, pp. 1591–1594, 2014, doi: 10.1109/EMBC.2014.6943908.

[47] T. G. Oesterlein *et al.*, "Analysis and visualization of intracardiac electrograms in diagnosis and research: Concept and application of KaPAVIE," *Comput. Methods Programs Biomed.*, vol. 127, pp. 165–173, 2016, doi: 10.1016/j.cmpb.2015.12.007.

[48] C. S. Elayi *et al.*, "Atrial fibrillation termination as a procedural endpoint during ablation in long-standing persistent atrial fibrillation," *Hear. Rhythm*, vol. 7, no. 9, pp. 1216–1223, 2010, doi: 10.1016/j.hrthm.2010.01.038.

[49] A. Verma *et al.*, "Approaches to catheter ablation for persistent atrial

fibrillation.," *N. Engl. J. Med.*, vol. 372, no. 19, p. 1812, doi: 10.1056/NEJMoa1408288.

[50] E. M. Annoni, S. P. Arunachalam, S. Kapa, S. K. Mulpuru, P. A. Friedman, and E. G. Tolkacheva, "Novel Quantitative Analytical Approaches for Rotor Identification and Associated Implications for Mapping," *IEEE Trans. Biomed. Eng.*, vol. 65, no. 2, pp. 273–281, doi: 10.1109/TBME.2017.2763460.

[51] R. Oakes *et al.*, "Detection and Quantification of Left Atrial Structural Remodeling With Delayed-Enhancement Magnetic Resonance Imaging in Patients With Atrial Fibrillation," *Circulation*, vol. 119, no. 13, pp. 1758-U123, doi: 10.1161/CIRCULATIONAHA.108.811877.

[52] N. F. Marrouche *et al.*, "Association of Atrial Tissue Fibrosis Identified by Delayed Enhancement MRI and Atrial Fibrillation Catheter Ablation: The DECAAF Study," *JAMA*, vol. 311, no. 5, pp. 498–506, doi: 10.1001/jama.2014.3.

[53] B. Scherr *et al.*, "Five-Year Outcome of Catheter Ablation of Persistent Atrial Fibrillation Using Termination of Atrial Fibrillation as a Procedural Endpoint," *Circ. Arrhythmia Electrophysiol.*, vol. 8, no. 1, pp. 18–24, doi: 10.1161/CIRCEP.114.001943.

[54] J. Xu *et al.*, "Atrial Extracellular Matrix Remodeling and the Maintenance of Atrial Fibrillation," *Circ. J. Am. Hear. Assoc.*, vol. 109, no. 3, pp. 363–368, doi: 10.1161/01.CIR.0000109495.02213.52.

[55] L. Tanaka *et al.*, "Spatial Distribution of Fibrosis Governs Fibrillation Wave Dynamics in the Posterior Left Atrium During Heart Failure," *Circ. Res.*, vol.

101, no. 8, pp. 839–847, doi: 10.1161/CIRCRESAHA.107.153858.